Local and global behavior of walls with cut-out openings in multi-story reinforced concrete buildings

Cristian Sabau[1,*]; Cosmin Popescu[2]; Niklas Bagge[3]; Gabriel Sas[4]; Thomas Blanksvärd[4]; and Björn Täljsten[5]

[1]Ph.D. Candidate, Dept. of Civil, Environmental and Natural Resources Engineering, Luleå Univ. of Technology, 971 87, Luleå, Sweden.

*(corresponding author) E-mail: cristian.sabau@ltu.se

[2]Researcher, Northern Research Institute – NORUT, Rombaksveien E6-47, N-8517 Narvik, Norway.

[3]Structural Engineer, Dept. of Bridge and Hydraulic Design, WSP Sverige AB, 40251, Gothenburg, Sweden.

[4]Associate Professor, Dept. of Civil, Environmental and Natural Resources Engineering, Luleå Univ. of Technology, 971 87, Luleå, Sweden.

[5]Associate Professor, Dept. of Civil, Environmental and Natural Resources Engineering, Luleå Univ. of Technology, 971 87, Luleå, Sweden.

[6]Professor, Dept. of Civil, Environmental and Natural Resources Engineering, Luleå Univ. of Technology, 971 87, Luleå, Sweden.

Abstract

This paper presents the finite element analysis (FEA) results of a multi-story reinforced concrete (RC) building having precast and cast-in-place load bearing walls. Door-type cut-out openings (height: 2.1 m, width: 0.9–4.4 m) were created at the first and second story of the building. Results from experimental tests on axially loaded RC panels were used to verify the modeling approach. The influence of cut-out openings on the response of individual RC panels, failure modes, and load redistribution to adjacent members under increasing gravitational loads was analyzed. Moreover, the wall bearing capacities obtained from FEA were compared with the values calculated from design equations. The results revealed that the robustness of multi-story buildings having RC load bearing wall systems decrease considerably with the creation of cut-out openings. However, owing to the initial robustness of the buildings, large cut-out openings could be created under normal service conditions without strengthening of the building structure. Furthermore, design equations provided very conservative predictions of the ultimate axial capacity characterizing the solid walls and walls with small openings, whereas similar FEA and analytically predicted capacities were obtained for walls with large openings.

Keywords: reinforced concrete; cut-out openings; push-down analysis; robustness; finite element analysis; nonlinear static analysis; load-bearing walls.

1. Introduction

Interventions to existing reinforced concrete (RC) buildings having precast and cast-in-place load bearing wall panels are common due to, for example, changes in the use and/or function (e.g., conversions of apartment buildings to office spaces). The new functionality usually requires increased amount of space as well as redesign and, hence, improved space efficiency of the building. Often, this means cutting new openings: starting from a regular door opening up to the point where an entire wall must be removed. These actions will inevitably damage the structure by affecting both the serviceability (admissible stresses, crack widths, and deflections) and the ultimate (i.e., load-carrying capacity) limit states.

The topic of openings in structural panels has been previously investigated via experimental and numerical methods [1-3]. Most of the studies have focused on the design aspects of walls with appropriate reinforcement detailing around the edges of the openings, as required in design codes [4, 5]. However, when openings are introduced into existing buildings, proper reinforcement detailing around the corner of the openings is lacking. This issue has rarely been considered [6-11]. Previous experimental studies focused on the effect of cut-out openings in large elements have shown that these openings are a source of weakness and can size-dependently reduce the structural stiffness and load-carrying capacity of a building. In all cases, repair and strengthening measures, using the use of fiber-reinforced composite materials, were proposed with the aim of restoring the specimen capacity to the pre-opening level. This approach is valid from a research point of view, but the studies focused on the component level [10, 12-14] rather than on the system level, i.e., the entire building.

In practice, a robustly designed building is characterized by important additional capacities due to the membrane effect and the redistribution of load effects to adjacent members. In the context of structural performance, structural robustness indicates the capacity of a building system to withstand the loss of local load-carrying capacity. At the structural level, cut-out openings can be assimilated into element removal scenarios. The robustness of building systems subjected to element removal, such as column loss due to impact or explosions, has typically been assessed through numerical, and analytical strategies (see, for example, [15]). However, previous studies quantifying the performance of building systems under gravity loads have focused mainly on steel or RC frame systems, and studies considering the building systems of RC panels are lacking.

The design and axial capacity assessment of RC walls in current standards [4, 5, 16, 17], is based on empirical models and calibration against the results of non-linear analysis. Compared with experimental results, these models provide overly conservative results, especially for walls with openings [1].

In this work, the influence of cut-out openings on the performance of multi-story residential buildings having a RC wall structural system is investigated. The performance of the building, in terms of maximum serviceability load, ultimate capacity, and robustness, is evaluated through non-linear three-dimensional (3D) finite element (FE) analysis. The adequacy of the modeling strategy is first validated at the component level, by comparing the numerical results with the experimental results obtained at Luleå University of Technology. The modeling approach validate using experimental tests on reinforced concrete walls is then applied at the structural level. Furthermore, the FEM results are compared with the results provided by the design guidelines.

2. Archetype building

The analyzed structure is an existing 11-storey residential building (Fig. 1), located in Romania, with the vertical load bearing system consisting of precast and cast-in-place reinforced concrete wall panels. The architectural concept [18] was designed and subsequently put into practice in the 1970s in Romania in area with varied levels of seismic risk, including low-seismicity regions with a then-current peak ground acceleration of 0.03*g*. Apartment blocks with structural wall systems, represents a typical structure across Europe, where for example, these structures represent 40%, 49%, and 45% of the residential building stock in Slovakia, Poland, and Estonia, respectively [19]. Important differences between the structured built in low or high-seismic regions was the amount and detailing of the steel reinforcement. For buildings in high seismic area the steel reinforcement in the concrete walls was designed such that walls panels withstand lateral shear forces and overturning moments, whereas in low seismic regions, walls were provided a minimum percentage of reinforcement to prevent cracking due to shrinkage or transportation.

The structural system consists of an integral wall system in which load-bearing walls run in both the longitudinal and transversal directions of the building. Structural simplicity is achieved by a regular floor layout, which runs from the foundation to the top of the building (see Fig. 2 for the layout of the 1st floor). The geometric characteristics of the structural elements are summarized below (the material properties of the structural elements are given in Table 1):

a) Walls. Two types of load-bearing walls carry the loads: cast-in-situ RC walls (Fig. 3) and prefabricated sandwich panels (Fig. 4a). The 150-mm-thick monolithic RC walls are used as interior walls ending with a 170-mm-thick flange toward the edge. The connection with the prefabricated outer walls is realized by casting the flange in a second stage. Each of these outer walls is a three-layer panel (including 70 mm, 60 mm, and 140 mm of protective layer, insulating material, and structural concrete, respectively) used to close the building envelope. In the current analysis, these walls are represented only by the structurally RC layer.

b) Floors. The floor panels (Fig. 4b) are prefabricated with a thickness of 120 mm, with top reinforcement anchored over the support. A steel wire mesh is used as the bottom reinforcement.

c) Joints and intersections. Shear stresses are transferred by the joints between external and internal walls through shear keys and welded lap splices, as shown in Fig. 5a–b. At the junction wall-floors, the stresses are transferred by a tie beam. The connection is realized through lap splices and shear keys, as shown in Fig. 5c–d.

3. Analysis method

The loads in the current analysis (shown in Table 2) are evaluated in accordance with EC 1 [20], although they might differ from the loads stipulated by previous standards used to design the building. In complex cases, simple analytical calculations are inadequate for determining the reliability of a given structure, but design codes offer the possibility of performing a load test [5]. Load testing a real structure is costly, time consuming, and limits the use of the structure. Numerical simulations of a load test are easier and less expensive than real tests. However, a FE analysis is typically performed prior to the test, and the test results are then used to verify and calibrate the model. Nevertheless, the present study considers only a FE-analysis of the building tests. The ACI 318 [5] standard provides a procedure for determining if a structure is allowed to remain in service. From the load combinations proposed in ACI 318 [5] load combination given by Eq. (1) was used, as it yields the highest total load, thus, all subsequent analyses are performed with this combination as the nominal load.

$$P = 1.15D + 1.5L + 0.4(L_r \text{ or } S \text{ or } R) \quad (1)$$

where, D: dead load, L: imposed load, L_r: roof live load, S: snow load, and R: rain load. Analyses are conducted considering a change in the building function from a residential to an office building and, hence, an initial live load of 2.0 kN/m^2 is used. Cut-out openings are introduced in the wall panel located along axis D and between axes 1 and 2 (this panel is referred to as wall D12, see Fig. 2). After the openings are created, a nominal live load

of 5.0 kN/m^2, corresponding to the live load for an office building. The serviceability of the building is subsequently evaluated.

Afterward, pushdown analysis is performed using the bay pushdown (BP) method [21], where the gravity load is increased proportionally only in the critical bays, i.e., the regions adjacent to the damaged element, until collapse occurs. The term damage (in this case) can refer to the complete or partial loss of the carrying capacity of a structural member. The remaining part of the structure is only subjected to nominal gravity loads. In a uniform pushdown analysis, the load is increased over the entire story and failure can occur in the weakest part of the structure, which may lie outside the critical bay. However, in BP, the collapse will correspond to the failure of the critical bay. Evidence of failure includes cracking, spalling, or large deflections. The capacity of the structure can be expressed in terms of the overload factor (OF), i.e., the ratio of the failure load and the nominal (design) gravity loads. The residual capacity (excess capacity) and possible collapse modes can be assessed through OF determination.

4. Failure criteria

A general acceptance criterion for the behaviour of a structure under loading is that this structure must resist failure. For example, according to ACI 318 [5], a building can remain in service at a certain load level or be decommissioned, based on evidence of failure, which is investigated in terms of: spalling or crushing of the concrete, reinforcement, anchorage slip, crack widths, and deflections affecting the function of the building. Therefore, regarding failure, two performance levels can be defined as follows:

Serviceability level: In accordance with ACI 318 [5], the acceptance criteria are specified in terms of deflections and crack openings, with acceptable deflections of structural elements under proof loading given as:

$$\Delta = \frac{l^2}{20000t} \tag{2}$$

Where, l is the span of the member and t is the member thickness.

According to EC 2 [4], the appearance and general utility of a structure can be impaired if the deflection of structural components exceeds the span/250. This standard also suggests that an appropriate limit for element deflection after construction under quasi-permanent loads can be calculated as: $\Delta = l/500$. From Eq. (2), a Δ of

4.1 mm is obtained based on the geometries of slabs C and E. In this case, ACI 318 [5] provides a more conservative limit (than EC 2 [4], i.e. 21 mm), which will be used as the deflection serviceability limit.

Acceptance criteria for the wall panels are set in accordance with ACI 533 [22], which stipulates maximum allowable crack widths and deflections of 0.3 mm and H/260, respectively (H: height of wall), for normal service conditions. According to ACI 533 [22], under normal service conditions, cracks up to 0.3 mm wide are structurally acceptable in precast wall panels. This limitation is consistent with the provision for the exposure classes (except for classes X0 and X1, where the limit is 0.4 mm) described in EC 2 [4]. A crack opening size of 0.3 mm will be used as the crack opening serviceability limit.

Ultimate level: The ultimate limit state concerns the safety of people and the ability of the structure to carry the imposed loads. Exceeding the ultimate load level implies total or partial collapse of the structure. However, failure involves the collapse of the element, excessive deformation (i.e., concrete crushing), and yielding of the reinforcement (i.e., large cracks occur).

According to EC 2 [4], limit states prior to structural collapse can be considered rather than the collapse itself and may be treated as the ultimate limit state. The loss of equilibrium and failure via excessive deformation or rupture represent relevant limit states that must be verified for an entire structure or part of a structure. For concrete, deformations exceeding the value associated with concrete crushing are considered excessive. The concrete strain at peak stress can be determined in accordance with EC 2 [4], where:

$$\varepsilon_{cu} = 0.7 f_c^{0.31} \quad (3)$$

with f_c: concrete compressive strength.

For the wall elements in this study, the total strain at the compressive strength of ε_{cu}=1500 μm/m is used to determine the initiation of concrete crushing. Excessive deformation of the reinforcement occur beyond yielding of the material. For the wall reinforcement used in the FE model, the yielding strain is ε_y=1200 μm/m, which is determined from the design yield stress and the modulus of elasticity (210 GPa).

5. Numerical model

5.1 Model Description

The FE analysis is performed using the ATENA Studio software package [23]. FE models of the archetype building and the experimentally tested panels are created using (in general) the same modeling strategy. Unless

otherwise stated, the description provided in this chapter is valid for both the building model and the models of the experimentally tested walls.

To manage the required computational effort, the FE size is varied depending on the structural element and its expected behavior during loading. However, in all cases, the concrete is modeled using 3D continuum isoparametric brick elements having 8-nodes. The steel reinforcement is modeled either as embedded bars in the concrete using 2-node truss elements or smeared layers of elements with nodes connected to those of the concrete elements. More specifically, the reinforcement of the first- and second-story wall and slab panels of the critical bay are modeled discretely, whereas the reinforcement in the joints and tie beams is smeared.

5.2 Material models

A non-linear concrete material model (i.e., CC3DNonLinCemetitious in Atena) is used for structural elements of the critical bay, whereas, to reduce the computational effort, a linear elastic model is employed for all other elements. The non-linear material model used for the concrete response is a fracture-plastic model that combines constitutive models for tensile (fracture) and compressive behavior (plastic) [24]. An orthotropic smeared crack model based on the Rankine tensile criterion and the yield surface proposed by Menetrey and William [25] are employed for concrete cracking and concrete crushing, respectively. The tensile response of the concrete is assumed to be linear-elastic up to the peak value of the tensile strength, f_t. The corresponding initial elastic modulus of the concrete and the strain at this state are E_c and $\varepsilon_t=f_t/E_c$, respectively. After the tensile strength is reached, tension softening is represented by a fictitious crack model based on a crack-opening law and fracture energy in combination with the crack band approach (Fig. 6a). The fixed crack model is employed in the present study. According to Reinhardt et al. [26], crack opening is governed by:

$$\sigma = f_t \left\{ \left[1+\left(c_1 \frac{w}{w_c} \right)^3 \right] \exp\left(-c_2 \frac{w}{w_c} \right) - \frac{w}{w_c}\left(1+c_1^3\right)\exp\left(-c_2\right) \right\} \quad (4)$$

Where, w: crack opening, w_c: crack opening at the complete release of stress, σ: normal stress in the crack, c_1=3 and c_2=6.93 are material constants.

The shape function of the concrete in compression (Fig. 6b) is derived from the work of van Mier [27]. Furthermore, the hardening law for concrete in compression is expressed through an elliptic function of the strains:

$$\sigma_c = f_{c0} + \left(f_c - f_{c0}\right)\sqrt{1-\left(\frac{\varepsilon_c - \varepsilon_{eq}^{p}}{\varepsilon_c}\right)^2} \quad (5)$$

Where, f_{c0}: onset of non-linear behavior, f_c: compressive strength of concrete, and ε_{eq}^{p}: equivalent plastic strain. To avoid mesh dependency, the softening law governing compression results in linearly descending trends with the end of the curve defined via the plastic displacement w_d. The default plastic displacement, w_d=*0.8* mm, is used. In this study, other concrete parameters such as the tensile strength (f_t), fracture energy (G_f), and modulus of elasticity (E_c), are evaluated as a function of f_c, using the formulas in Table 3.

For the reinforcement modeled as discrete bars (i.e., the reinforcement of the critical bay elements and the reinforcement considered in the experimental tests) the interaction between the bar and the surrounding concrete is considered using the Model Code 2010 [28] bond law. For the smeared reinforcement, a perfect bond between the concrete and reinforcement is assumed. The uniaxial stress state of the reinforcement is defined using a simplified multi-linear model in accordance with the stress-strain properties of the experimentally tested steel reinforcement coupons and the design specification of the archetype building.

The modified Newton-Raphson iterative scheme with error tolerances of 1%, 1%, and 0.01% corresponding to the displacement, residual force, and energy (i.e., convergence criteria), respectively, is used to obtain the solution for each load increment.

5.3 Model verification

The adopted numerical modeling technique is validated for simulating the non-linear behavior of axially loaded RC walls with openings. The numerical results obtained for the RC panel with and without openings are compared with the experimental test results.

5.3.1 *Experimental investigation*

Half-scale walls representing typical wall panels in residential buildings (1.8 m × 1.35 m × 0.06 m) with and without cut-out openings, are constructed for testing to failure. The experimental program includes walls with symmetric openings that replicate solid walls with sawn cut-outs, i.e., no additional reinforcement is placed around the edges or corners of the openings.

The test matrix consists of three walls, namely a: solid wall (SW), wall with a symmetric half-scaled single door-type opening (450 × 1050 mm; SO), and wall with a symmetric half-scaled double door-type opening (900 × 1050 mm; LO). Welded wire fabric reinforcement, consisting of deformed 5-mm-diameter bars with 100-mm spacing in both orthogonal directions and centrally placed in a single layer, was used to reinforce the walls. The dimensions and detailing of the specimens are shown in Fig. 7a, with the material properties (average values from material tests) summarized in Table 4.

The specimens are all cast as solid panels, i.e., with constant thickness, no voids, and no insulating layers, and designed to carry vertical loads without lateral in-plane forces or transverse loads between the supports. The walls are subjected to axial loading with a small eccentricity along the weak axis (1/6 of the wall thickness), to represent imperfections due to thickness variations and panel misalignment during the construction process. To ensure a uniform distributed load along the length of the wall, four hydraulic jacks are networked together to transmit the forces to the wall through a loading beam (excluded from Fig. 7b to improve visualization of the test setup). The specimens are tested in two-way action; side edges are restrained to simulate real transverse walls in a structure allowing rotation, but preventing translation. The top and bottom boundaries of the specimen were hinged connections that permit free rotation. Additional details about the experimental program are provided by Popescu et al. [10].

Linear displacement transducers are used to monitor the out-of-plane displacements *(δ)* of each tested specimen and a 3D optical deformation measurement system (Aramis 5M) commonly referred to as a digital image correlation (DIC) system, was used to determine the principal tensile strain distribution around the upper-right corner on the tension side of the specimen (approximately *780 mm × 660 mm*). The setup used for these measurements is described in Sabau et al. [29].

5.3.2 *Finite element modeling of experimental tests*

Realistic (insofar as current knowledge permits) behavior should be modeled for all materials and boundary conditions, thereby verifying that the chosen modeling approach is adequate in representing the behavior of axially loaded wall panels. Based on the symmetry of the test setup, only half of each specimen is modeled. The boundary conditions and loading scheme are imposed in accordance with the tests. The self-weight of the specimen is included in the model, and line supports are used to simulate the supports. Similar to the experimental setup, to

avoid stress concentrations, linear elastic steel plates (comprising the region between wall edges and the loading and support points) are added to the model. To simulate the experimental conditions, the bottom line support is restrained in the vertical, horizontal, and out-of-plane directions, whereas the top and lateral supports are restrained in the horizontal and out-of-plane directions only. A static non-linear analysis is performed by applying an incremental vertical displacement of the top loading line. The positions of the loading line and bottom support line are set to match the eccentricity associated with the experimental tests.

Considering the computation time and numerical accuracy, the mesh is generated using structured elements with an aspect ratio of *1:2:2* (thickness: length: height), where the unit corresponds to the thickness direction of the wall. The wall thickness is divided into six elements, thereby yielding a fine $10 \times 20 \times 20\ mm$ mesh.

5.3.3 *Adequacy of the FE model*

The FE model should provide an adequate description of the global behavior and failure mode of RC walls. To check the level of adequacy, the load-displacement response and tensile strain distribution at failure obtained from the FE analysis are compared with those from the experimental tests, as shown in Fig. 8.

Local measurement results may deviate from the global behavior characterizing a structural element, owing to the occurrence of stress concentrations or cracks (which may occur in places other than the sensor locations). Therefore, the adequacy of the model is verified based on the error in predicting the ultimate load as well as the ability to reproduce the experimentally observed deformations and crack patterns. A value of 0.96 (average error: <4%) is obtained for the average ratio of the numerical and experimental ultimate loads.

Furthermore, the comparison is made based on the surface strain distribution that is representative of the crack pattern in concrete elements [30]. The principal tensile strain components at failure of the panels with openings, relative to the outline of each specimen, is shown in Fig. 8b. The distributions obtained from the FE model and the DIC system are shown on the left and the right, respectively. The close correspondence between the principal strain distributions indicates that the experimentally observed deformation and crack patterns are adequately reproduced by the FE model, confirming the similarity between the boundary conditions of the two cases.

5.4 Building model and analysis setup

Fig. 9 shows an overview of the FE model of the building, for which the first 3 stories were explicitly modeled, and the discretization used for the members in the critical bay. The critical bay represents the section of the building

that will most likely be affected by the creation of cut-out openings (see Fig. 2). The critical bay consists of the following members: the wall with the cut-out opening (i.e., wall D12); the adjacent transversal walls, 1BD, 1DF, 2DB, and 2DF; the slabs of bays C and E.

For the wall with cut-out openings, i.e., wall D12, the wall thickness is divided into six elements and is assigned finite elements with an aspect ratio of 1:2:2 (thickness: length: height), similar to the tested walls. To reduce the computational effort, other members of the critical bay are assigned elements with a maximum aspect ratio of 1:4:4. In all cases, a minimum of five elements are spread over the thickness of the structural element, as recommended by [31], to avoid "shear locking". The rest of the structure is modeled using only one numerical element per thickness and maintaining the aspect ratio (1:4:4) of the elements.

The first- and second-story members of the critical bay are assigned non-linear material properties, whereas, to save computation time, the remaining sections of the building (including the entire third story) are assigned linear elastic material properties. A preliminary study performed by the authors [32], focused on modeling the slabs of the critical bay using non-linear properties up to failure. The results indicated that the load-carrying capacity of the building without openings is limited mainly by the capacity of the slabs. However, several studies have shown that the capacity of RC slabs can be considerably increased via strengthening [8, 33-36]. The present study focuses on the behavior of RC walls and, hence, slab strengthening to a capacity beyond that associated with failure of the other members is assumed. Therefore, after the serviceability load level is reached, failure of the wall panel is promoted by assigning linear-elastic material properties to each slab in the critical bay. Thus, for serviceability-related analyses and the pushdown analysis, slabs are assigned non-linear material models and linear elastic material models, respectively.

Imperfections occur in normal construction practices generally within tolerance limits specified construction guidelines such as [37]. In the analysis, the effects of these imperfections are included by introducing eccentricities for the critical elements. Walls D12, 1BF, and 2BF are provided with an out-of-plane eccentricity equivalent to a sixth of the member thickness, (i.e., $e = t/6$) at the first story, the same as that used in the experimental tests. This implies that wall panels can be treated as compression members [38], as the resultant of forces acting at the boundaries of the member passes through the middle third of the section, enabling further comparison with equations recommended in design guidelines.

The first three stories are explicitly modeled considering the building in the original (AsBuilt) state (i.e., without cut-out openings). The factored dead, imposed, and live (2.0 kN/m^2) loads are applied to each story. For the 3rd story, loads are multiplied by a factor of 9, representing the number of stories excluded from the analysis. Once all loads are applied, concrete and reinforcement elements corresponding to cut-out openings are deleted at the first and/or second story. The live load is then increased by 3.0 kN/m^2, as per the change of function scenario, and the bay pushdown is performed.

This procedure is applied to buildings having door-type cut-out openings of sizes indicated in Table 5. Openings are created in wall D12 (see Fig. 2) at the first and second story, referred to as 1st and 2st, respectively. To facilitate subsequent discussions, each analysis case is designated as "Building Oxy", where x and y (with values ranging from 1 to 4) represent the size of the opening created at 1st and 2st, respectively, as indicated in Table 5.

For example, Building O23 represents a building with opening O2 (size: 1.6 m × 2.1 m) at the first story and opening O3 (size: 3.0 m × 2.1 m) at the second story; Building AsBuilt represents the building without any cut-out openings (see Table 6 for a summary of the model names based on the opening configuration).

The total base reaction of the building is monitored. The individual reactions of walls 1BD, 1DF, 2BD, 2BF, and D12 are also monitored during the FEM analyses, with the sum of these reactions representing the total load distributed to the critical bay. Similarly, the maximum concrete compressive strain, reinforcement tensile strain, and out-of-plane displacement are monitored for each panel.

6. Results and Discussion

6.1 Response of wall panels with cut-out openings

Fig. 10 shows the axial load-maximum out-of-plane displacement response of wall D12 at the first and second story for different sizes of openings created at the first story. The maximum out-of-plane displacement was recorded approximately at mid-height of the panel, in the panel center for the solid wall, and at the free edge of the pier for the walls with openings. The compressive strain distribution and crack pattern at the ultimate load on the face viewed from Slab E, are also shown in the figure. Similarly, Fig. 11–14 show the load response as well as the strain and crack distribution of wall D12 with openings in the second-story panel.

The wall load-displacement response for the AsBuilt, O10, and O20 cases is similar to the experimentally determined response (see Fig. 8 and Fig. 10). As shown in Fig. 10, the axial capacity decreases significantly with

increasing opening size. Failure of the (i) second-story panel in the AsBuilt building occurs via concrete crushing at the bottom edge of the panel and (ii) first-story panel (i.e., the one with the cut-out opening) in the O10 and O20 cases occurs first. The compressive strain distributions revealed that failure occurred first for the pier adjacent to the outer walls of the building. Popescu et al. [10] and Sabau et al. [11] determined, via experiments, that for panels with openings, failure of the piers is non-simultaneous, and occurs first in the panel experiencing the highest out-of-plane displacements. Moreover, full-field measurement on tested walls revealed that the distributions of compressive strain for the solid panel and panels with openings are similar to those obtained from the FEA.

For buildings O30 and O40, the crack pattern suggests that the solid panel at the second story undergoes shear failure. Moreover, for openings O3 and O4 (which are larger than 3 m) at the first story, shear failure occurs in the second-story panel with openings, except for cases where the same opening width is used at both stories.

The maximum axial load for wall D12 and the maximum load applied to the slabs of the critical bay of each analyzed building are given in Table 7 and Table 8, respectively. As the Table 7 shows, the cut-out opening-induced decrease in the axial load in the wall is non-proportional to the decrease in load-carrying capacity of the building. Consider the cases of a 0.9-m and 4.4-m wide opening (door), compared to the AsBuilt case, the maximum load carried by the wall decreases by 14% and 86%, respectively, whereas the load-carrying capacity of the building decreases by 4% and 70%, respectively. The capacity decrease is therefore more pronounced at the element level than at the system structural level. Moreover, this difference is more significant for smaller openings (0.9 m–1.6 m) than for larger openings (3.0 m–4.4 m). For a robustly designed building, the additional capacities due to the membrane effect and the redistribution of forces to adjacent members limit the cut-out opening-induced decrease in the building capacity.

6.2 Influence of openings on the load redistribution to foundations

Previous experimental tests have shown that the capacity and the stiffness of solid concrete panels decrease considerably when cut-out openings are created [10]. At a structural level, such changes can alter the path of loads in the structures and can lead to higher loads (than the original set of loads) distributed to other elements.

The influence of openings on the axial load distribution between the vertical wall panels is determined from changes in the total reaction forces at the bottom support of each wall. These forces represent the loads transmitted to the foundation by the wall panels.

Fig. 15 shows the reaction coefficient (i.e., the reaction of a wall divided by the total reaction in the critical bay) of walls 1BD, 1DF, 2BD, 2BF, and D12 for different opening configurations. Fig. 15 a) to e) show the influence of enlarging an opening of the first story when the wall on the second story is solid or has openings of different sizes.

The axial load transmitted by wall D12 decreases with increasing size of the opening, whereas the load in the adjacent wall increases. For example, in the case of Building O40 the reaction force of wall D12 is ~62% lower than that of the AsBuilt Building, whereas the force of wall 1BD is ~60% higher. This indicates that loads are proportionally redistributed to adjacent members, owing to the creation of openings and the corresponding change in the wall axial rigidity. Thus, in practical cases of such interventions, the conditions characterizing the foundations must be investigated.

6.3 Influence of openings on adjacent stories

The location of the cut-out opening at the first or the second story influences the maximum load carried by the wall, as well as the maximum load-carrying capacity of the building, the results are summarized in Table 7 and Table 8, respectively. For a manageable computational effort, structural elements considered of secondary importance to the performed analysis were modeled with a lower degree of detailing. Wall panel D12 (at the third story), which was expected to mainly to distribute forces to the second story, was considered non-critical for the analysis and, is assigned linear-elastic material properties, thus the shear capacity of this panel might was overestimated. This led to higher capacities for the same kind of openings at the second story compared to the first story. Consider, for example the reduction in the axial capacity of wall D12, compared to the AsBuilt case the reduction is 86% for case O40, but only 52% for the same opening at the second story (i.e., O04). Moreover, because shear failure in the third story panel is prevented it can redistribute loads to adjacent members. Therefore, the maximum applied load decreases by 70% and 8% for cases O40 and O04, respectively.

This indicates that the boundary conditions and the behavior of the adjacent members, significantly influence the load carried by a wall. Moreover, the choice of material model exerts considerable influence on the capacity of the structure. Detailed modeling should therefore be performed (i) by employing a non-linear concrete material model for third-story panels corresponding to second-story panels with large openings and (ii) for the elements

adjacent to the panels with openings, thereby allowing identification of the failure mode corresponding to the lowest load level.

Cutting-out same size openings at the first and second story yields a similar decrease in load capacity to that observed when an opening is created only at the first story (Table 7). For large openings at the first story and smaller openings at the second story, the second-story panel (in general) undergoes shear failure at lower load levels than those leading to the failure of same-size openings. When large cut-out openings are required in two adjacent stories, shear failure can be prevented by using the same opening size at both stories; if different sizes are employed, the shear capacity of the above-situated panel must be verified.

6.4 Influence of openings on serviceability and ultimate level performance

The influence of openings on the serviceability (total live load: 5.0 kN/m^2) is first assessed under the load combination described by Eq. (1). The out-of-plane deflection of each panel in the critical bay, vertical displacement of the spandrel composing the opening, and vertical deflection of the slabs are compared with the respective allowable values defined in Section 4. For all opening configurations, the maximum deflections under the serviceability load combination are considerably lower than the recommended limits. For example, the maximum deflection of the spandrel in the O44 case and the allowable deflection determined from Eq. (2) are ~0.25 mm and 1.3 mm, respectively.

The maximum deflection of the slab comprising the O44 building is 0.75 mm, well below the 4.1 mm allowable deflection determined from Eq. (2). The maximum displacements of the slabs comprising the first story of the AsBuilt is 0.50 mm. Therefore a 50% increase slabs' deflection under the service load is attributed to the creation of the cut-out openings.

Tables 9 to 12 show the load bearing capacity of the building for the serviceability (i.e., crack width) and ultimate limit state conditions determined by the initiation of concrete crushing ($\varepsilon_c \geq 1484$ μm/m) and yielding of the reinforcement ($\varepsilon_y \geq 1231$ μm/m).

Table 9 shows the applied load where cracks larger than 0.3 mm open in one of the walls comprising the critical bay. For cases with larger openings at the first story than at the second story, cracks appear first at the bottom of the second-story wall. Shear cracks and flexural cracks then occur in the second-story wall and spandrel of the first-story wall, respectively. For cases with smaller openings at the first story than the second story, flexural cracks

appear first in the spandrel of the second-story wall. Furthermore, an additional characteristic live load of 15–33 kN/m^2 (see Table 10) can be applied to the slabs of the critical bay before the serviceability limits characterizing the concrete wall are exceeded.

Tables 11 and 12 show the applied load associated with concrete crushing and reinforcement yielding, respectively. With the exception of Buildings O43 and O44, concrete crushing is initiated prior to yielding of the reinforcement in each building.

The OFs of each analyzed building are shown in Table 13. These factors are determined as the ratio of the characteristic live load from the pushdown analysis, corresponding to concrete crushing and reinforcement yielding, and the design live load (i.e., 5.0 kN/m^2). To avoid structural failure, the OFs must be greater than or equal to unity. The obtained OFs indicate that the buildings are quite robust and can potentially accommodate openings of considerable sizes. The OFs in Table 13 range from 4.1 to 11.7, with the highest and lowest values occurring for the AsBuilt building and the buildings with the largest openings, respectively.

Previous studies on buildings having seismically designed moment-resisting frame systems under column removal scenarios [21, 39], have reported OFs ranging from 1.4 to 3.6. Thus, buildings having wall structural systems are considerably more robust than frame systems. However, the building robustness decreases significantly with increasing size of the cut-out openings. The OFs of the largest opening sizes considered in the present study are similar to those obtained for frame structures, confirming that for large opening sizes, the structural behavior of RC panels is similar to that of RC frames.

6.5 Comparison with design equations

The ultimate load of wall D12 obtained from FEA for each model and the experimentally obtained loads for the tested panels are presented (see Fig. 16) in terms of the axial strength ratio and the opening size ratio. The axial strength ratio is defined as $N/t{\cdot}L{\cdot}f_c$, where N: axial load, t: wall thickness, L: total length of the wall, and f_c: mean concrete compressive strength. The opening size ratio is defined as L_0/L, where L_0 and L are the width of the opening and the total length of the wall, respectively. These ratios facilitate the comparison of elements having different concrete strengths and different sizes and, in turn, the influence of openings on the ultimate load can be determined.

The axial strength ratio obtained via FEA for the case with solid walls is ~2.5 times higher than the experimentally obtained ratio. However, the wall boundary conditions imposed in the calculations differed from those of the experiments. In the experimental tests, the panels are provided with pinned supports, whereas for the analyzed building, the detailing at the intersections between panels allows flexural moments at the panel edges. Therefore, in the FEA, the connection between each panel (rather than acting as pinned supports) exhibits flexural rigidity. In both cases, the axial strength ratio decreases almost linearly with the opening size (the decrease is higher for the flexurally rigid case than for the pinned supports, as indicated by the slope of the best-fit line).

According to EC 2 [4], the ultimate capacity of the solid RC walls can be determined from:

$$N = f_c \cdot L \cdot t \cdot \Phi \tag{6}$$

Where, Φ is the axial strength ratio, i.e., the factor accounting for the influence of the eccentricity, aspect ratio, and boundary conditions:

$$\Phi = 1.14\left(1 - \frac{2(e_0 + e_i)}{t}\right) - 0.02\frac{H_{eff}}{t} \leq \left(1 - \frac{2(e_0 + e_i)}{t}\right) \tag{7}$$

Where, e_0: first-order eccentricity, e_i: additional eccentricity ($e_i = H_{eff}/400$) and $H_{eff} = k \cdot \beta \cdot H$: effective height of the member, where β, a coefficient accounting for the aspect ratio of the wall and the number of supports, is given as:

$$\beta = \begin{cases} 1 & for\ one-way\ walls\ supported\ on\ two\ edges \\ \dfrac{1}{1+(H/3L)^2} & for\ two-way\ walls\ supported\ on\ three\ edges \\ \dfrac{1}{1+(H/L)^2}\ if\ L \geq H & for\ two-way\ walls\ supported\ on\ four\ edges \\ H/2L \quad if\ L < H & \end{cases} \tag{8}$$

and k is the effective length factor for the support rotational restrains. According to EC 2 [4], k=1 and k=0.5 for isolated compression members with pinned supports and rotational rigid supports, respectively. However, for walls having flexurally rigid connections EC 2 [4] recommends that k may be taken as 0.85. Other codes such ACI318 and CSA-04, recommend that the k of OW walls may be taken as 0.8 and 0.75, respectively. The solid wall is considered as a two-way wall supported on four edges. For the walls with openings, the capacity of each pier (for a total of two piers) is calculated as two-way compression members supported on three edges, and the values are then summed.

Fig. 16 shows the L_0/L dependence of the axial strength ratio characterizing a RC wall calculated according to EC 2 [4], where pinned and rotational rigid supports (i.e., k=1 and k=0.5, respectively) are considered. For k=1, the axial strength factor is similar to the experimentally observed values. The decrease in the wall capacity relative to the opening size (as determined from the slope of the lines obtained via linear regression) is also similar to the experimental values. This is expected, since design models are usually calibrated based on experimental results corresponding to pinned support conditions.

Considering rotationally rigid, rather than pinned (i.e., k=0.5) supports, EC 2 [4] yields higher capacities than the FEA. This increase is inversely proportional to the opening size, and the influence exerted by the rotational stiffness of the support decreases with increasing opening size. However, higher axial strength ratios are obtained from the FEA (than from the EC 2) of the RC wall as part of the building. This is especially true for $L_0/L < 0.5$. The EC 2 [4] recommends a factor of k=0.85 and, thus, the contribution of rotationally rigid supports is greatly underestimated.

For opening size ratios >0.5, shear failure occurs in the panel above the cut-out opening. This behavior is similar to frame-like behavior, with the upper story wall acting as a deep beam, supported on the piers of the wall with the cut-out opening (see Fig. 10).

Moreover, EC 2 [4] specifies that elements with aspect ratio below 4:1 (L/t) should be designed as columns rather than walls. Considering the geometry of the simulated and tested walls, an L_0/L of ~0.75 yields an aspect ratio of 4:1 for the piers. A frame-type behavior is observed, however, even for walls with opening ratios of 0.5 (see Fig. 10). Thus, 0.5 can be taken as the critical value that distinguishes between small and large cut-out openings, representing the limit beyond which the wall-like behavior transforms into frame-like behavior.

7. Concluding remarks

Using Atena [18], a 3D finite element model is developed for an 11-story RC building. The building model is composed of wall and slab structural elements. The RC material properties and detailing used in the numerical model are obtained from the original design drawings. Results obtained from FEM analysis of the experimentally tested RC wall panels correspond closely to the experimentally determined ultimate capacity and deformation. In addition, the effect of cut-out openings on the behavior of a multi-story RC building is determined through a BP analysis.

The limited number of models analyzed indicate that door-type openings having widths of 0.5*the wall width and >0.5*the wall width can be considered small openings and large openings, respectively. For small openings, the structural behavior of the wall is similar to that of an axially loaded wall. However, for large openings, the behavior is similar to that of a frame, and additional checks for shear failures in the adjacent members are required as the occurrence of shear failure is likely.

Furthermore, the results obtained, where cut-out openings of widths exceeding 80% of the total panel width are created, suggest that multi-story buildings with RC structural walls can accommodate (i) cut-out openings of considerable size and (ii) a 3.0 kN/m^2 increase in the live load without exceeding the serviceability limits.

However, assumptions as well as limitations described in the paper include that structural elements were considered ideal (i.e., without pre-existing cracks or initial imperfections due to element curvature, and full restraints at the member joints are assumed). The structure of an existing building can, however, be weakened, owing to damage suffered during the service life of the building. Therefore, the results of this study are not directly applicable to existing structures, as in practice, a cases by case analysis needs to be performed for any building considering its structural condition. Moreover, further study is required to determine the influence of other eccentricities (such as the wall deviation from verticality, variation in the wall thickness, and pre-existing curvatures of the elements) on the structure of the building.

The robustness of the analyzed building is demonstrated by the high overload factors reached before the ultimate capacity of the structural walls is achieved. For the largest opening sizes used in this study, the building exhibits similar levels of robustness to seismically designed frame structures [21, 39]. However, the results revealed that, the buildings' robustness is significantly reduced by cut-out openings. Therefore, strengthening solutions aimed at limiting the loss of robustness should be further investigated.

The EC 2 [4] design guideline yields good predictions compared with the capacities obtained from experimental tests of the wall panels. However, compared with the results of the present FEA study, the ultimate loads predicted by EC 2 [4] are extremely conservative, especially for the case of solid walls and walls with small openings.

This study was focused on uniform distributed gravitational loads to a partial model of a structure created based on original design drawings. Further studies are required for determining the influence of lateral loading, such as

wind or seismic loads, and non-uniform gravitational loading (which may increase the effect of load eccentricity) on the structure.

Acknowledgment

This work was supported by the European Commission (Contract number MC-ITN-2013-607851) and Development Fund of the Swedish Construction Industry (SBUF). Dr. Sorin-Codruț Floruț from Politehnica University Timisoara is gratefully acknowledged for providing access to the original design plans of the studied building. The first author would like to acknowledge the support of the European Network for Durable Reinforcement and Rehabilitation Solutions (*endure*).

References

[1] Popescu C, Sas G, Blanksvärd T, Täljsten B. Concrete walls weakened by openings as compression members: A review. Engineering Structures. 2015;89:172-90.
[2] Ho N-M, Doh J-H, Fragomeni S. Instability analysis of reinforced concrete walls with various support conditions. The Structural Design of Tall and Special Buildings. 2017:e1353.
[3] Ho NM, Lima MM, Doh JH. Axially loaded three-side restrained reinforced concrete walls: A comparative study. Mechanics of Structures and Materials: Advancements and Challenges: CRC Press; 2016. p. 63-72.
[4] EC 2. Eurocode 2: Design of concrete structures. Brussels, B-1050, Belgium: European Committee for Standardization (CEN); 2005.
[5] ACI 318. Building Code Requirements for Structural Concrete. Farmington Hills, MI 48331: American Concrete Institute; 2011.
[6] Demeter I. Seismic retrofit of precast RC walls by externally bonded CFRP composites. Timisoara, Romania: Politehnica University of Timisoara; 2011.
[7] Mohammed BS, Ean LW, Malek MA. One way RC wall panels with openings strengthened with CFRP. Construction and Building Materials. 2013;40:575-83.
[8] Floruț S-C, Sas G, Popescu C, Stoian V. Tests on reinforced concrete slabs with cut-out openings strengthened with fibre-reinforced polymers. Composites Part B: Engineering. 2014;66:484-93.
[9] Todut C, Dan D, Stoian V. Numerical and experimental investigation on seismically damaged reinforced concrete wall panels retrofitted with FRP composites. Composite Structures. 2015;119(0):648-65.
[10] Popescu C, Sas G, Sabau C, Blanksvard T. Effect of Cut-Out Openings on the Axial Strength of Concrete Walls. Journal of Structural Engineering. 2016;142(11):04016100.
[11] Sabau C, Popescu C, Sas G, Blanksvärd T, Täljsten B. Axially loaded RC walls with cutout openings strengthened with FRCM composites. Journal of Composites for Construction. 2018;22(6):04018046.
[12] Doh JH, Fragomeni S. Ultimate load formula for reinforced concrete wall panels with openings. Advances in Structural Engineering. 2006;9(1):103-15.
[13] Fragomeni S, Doh JH, Lee DJ. Behavior of Axially Loaded Concrete Wall Panels with Openings: An Experimental Study. Advances in Structural Engineering. 2012;15(8):1345-58.
[14] Popescu C, Sas G, Blanksvärd T, Täljsten B. Concrete Walls with Cutout Openings Strengthened by FRP Confinement. Journal of Composites for Construction. 2017;21(3):04016106.

[15] De Biagi V, Parisi F, Asprone D, Chiaia B, Manfredi G. Collapse resistance assessment through the implementation of progressive damage in finite element codes. Engineering Structures. 2017;136:523-34.
[16] Standards Australia. Australian Standard for Concrete Structures. Sydney, Australia: Standards Australia; 2009.
[17] CSA S806. CSA S806. Design of concrete structures. Toronto, Canada: Canadian Standards Association; 2012.
[18] ISART. Residential buildings, category I, shear walls, P+10 floors, for 6th and 7th grade seismic regime Bucharest, Romania: Institutul de Studii si Proiectare pentru Sistematizare, Arhitectura si Tipizare (ISART); 1973.
[19] Csoknyai T, Hrabovszky-Horváth S, Georgiev Z, Jovanovic-Popovic M, Stankovic B, Villatoro O, et al. Building stock characteristics and energy performance of residential buildings in Eastern-European countries. Energy and Buildings. 2016;132:39-52.
[20] EC 1. Eurocode 1: Actions on structures. Brussels, Belgium: European Committee for Standardization; 2002.
[21] Khandelwal K, El-Tawil S. Pushdown resistance as a measure of robustness in progressive collapse analysis. Engineering Structures. 2011;33(9):2653-61.
[22] ACI 533. Guide for Precast Concrete Wall Panels. Farmington Hills, MI: American Concrete Institute; 2011.
[23] Cervenka Consulting. Atena version 5.6 Users Manual. 2018.
[24] Červenka J, Papanikolaou VK. Three dimensional combined fracture–plastic material model for concrete. International Journal of Plasticity. 2008;24(12):2192-220.
[25] Menetrey P, William KJ. Triaxial Failure Criterion for Concrete and its Generalization. ACI Structural Journal. 1995;92(3).
[26] Reinhardt HW, Cornelissen HAW, Hordijk DA. Tensile Tests and Failure Analysis of Concrete. Journal of Structural Engineering. 1986;112(11):2462-77.
[27] van Mier JGM. Multiaxial strain-softening of concrete. Mater Struct. 1986;19(3):179-90.
[28] Model Code 2010. Model Code for Concrete Structures 2010. Lausanne, Switzerland: Ernst & Sohn; 2013.
[29] Sabau C, Popescu C, Sas G, Blanksvärd T, Täljsten B. Monitoring structural behavior of reinforced concrete walls with openings using digital image correlation. In: Proceedings of 19th IABSE Congress. Stockholm, Sweden, Conference, Conference 2016. p. 1803-11.
[30] Ghorbani R, Matta F, Sutton MA. Full-Field Deformation Measurement and Crack Mapping on Confined Masonry Walls Using Digital Image Correlation. Experimental Mechanics. 2015;55(1):227-43.
[31] Hendriks MAN, de Boer A, Belletti B. Guidelines for Nonlinear Finite Element Analysis of Concrete Structures. Delft, Netherlands: Rijkswaterstaat Technisch Document (RTD); 2017.
[32] SBUF 13246. Rehabiliteringsmetoder för håltagning i armerade betongväggar. Skanska Sverige AB; 2018.
[33] Mostakhdemin Hosseini MR, Dias SJE, Barros JAO. Flexural strengthening of reinforced low strength concrete slabs using prestressed NSM CFRP laminates. Composites Part B: Engineering. 2016;90:14-29.
[34] Schladitz F, Frenzel M, Ehlig D, Curbach M. Bending load capacity of reinforced concrete slabs strengthened with textile reinforced concrete. Engineering Structures. 2012;40:317-26.
[35] Enochsson O, Lundqvist J, Täljsten B, Rusinowski P, Olofsson T. CFRP strengthened openings in two-way concrete slabs – An experimental and numerical study. Construction and Building Materials. 2007;21(4):810-26.

[36] Maazoun A, Belkassem B, Reymen B, Matthys S, Vantomme J, Lecompte D. Blast response of RC slabs with externally bonded reinforcement: Experimental and analytical verification. Composite Structures. 2018;200:246-57.
[37] Ascent. Envelope tolerances for architectural precast. Chicago: Precast/Prestressed Concrete Institute; 2012.
[38] Pillai SU, Parthasarathy CV. Ultimate strength and design of concrete walls. Building and Environment. 1977;12(1):25-9.
[39] Parisi F, Augenti N. Influence of seismic design criteria on blast resistance of RC framed buildings: A case study. Engineering Structures. 2012;44:78-93.

Figure captions

Fig. 1. Perspective view of the analyzed RC building.

Fig. 2. Floor plan layout.

Fig. 3. Reinforcement details of the cast-in-situ RC wall.

Fig. 4. Reinforcement details of the prefabricated RC elements: (a) outer wall; (b) floor panel.

Fig. 5. Joint details: (a) inner – outer walls (horizontal section); (b) inner – outer walls (vertical section); (c) prefabricated floor – wall panel (vertical section); (d) prefabricated floor – cast-in-situ RC wall.

Fig. 6. Constitutive model for concrete: (a) tensile softening; (b) compressive hardening/softening.

Fig. 7. Configuration of the tested walls: (a) details of the specimens; (b) schematic of test setup.

Fig. 8. Comparison of FEM analyses and experimental test results, a) load-displacement b) principal tensile strain distribution at failure for panels with openings.

Fig. 9. Finite element model of the analyzed building.

Fig. 10. Wall D12 out-of-plane displacement response for cases with the solid wall at the second story. The compressive strain and crack (>0.1 mm) distribution corresponding to the maximum load is shown.

Fig. 11. Wall D12 out-of-plane displacement response for cases with opening O1 (0.9×2.1 m) at the second story. The compressive strain and crack (>0.1 mm) distribution corresponding to the maximum load is shown.

Fig. 12. Wall D12 out-of-plane displacement response for cases with opening O2 (1.6×2.1 m) at the second story. The compressive strain and crack (>0.1 mm) distribution corresponding to the maximum load is shown.

Fig. 13. Wall D12 out-of-plane displacement response for cases with opening O3 (3.0×2.1 m) at the second story. The distribution of compressive strains and cracks (>0.1 mm) corresponding to the maximum load is shown.

Fig. 14. Wall D12 out-of-plane displacement response for cases with opening O4 (4.4×2.1 m) at the second story. The distribution of compressive strains and cracks (>0.1 mm) corresponding to the maximum load is shown.

Fig. 15. Comparison of wall reaction coefficients corresponding to a) the second-story solid wall, and second-story wall b) O1, c) O2, d) O3, and e) O4.

Fig. 16. Axial strength ratio versus L_0/L.

Tables

Table 1. Material characteristics

Structural element	Material quality	
	Concrete class	Reinforcement type
Prefabricated walls Prefabricated floors	B250 (f_{ck}≈16.6 MPa)	OB38 (plain bars f_{yk}≈235 MPa) and STM (welded wire mesh f_{yk}≈440 MPa)
Cast-in-situ walls (flange) Joints and intersections	B300 (f_{ck}≈20.5 MPa)	OB38 (plain bars f_{yk}≈235 MPa)
Cast-in-situ walls (web)	B200 (f_{ck}≈12.5 MPa)	OB38 (plain bars f_{yk}≈235 MPa)

Note: f_{ck} – characteristic concrete compressive strength
f_{yk} – characteristic reinforcement steel yield strength

621 **Table 2. Building loads**

Loads	Intensity
Dead load	
Self-weight	25 kN/m^3
Flooring	1.0 kN/m^2
Imposed load	
Live load	2.0 kN/m^2 or 5.0 kN/m^2
Roof live load	0.4 kN/m^2
Variable loads	
Snow	3.0 kN/m^2

622

623

624 **Table 3. Equations used to generate material parameters from the concrete compressive strength**

Parameter	Formula
Cylinder strength, f_c (MPa)	$f_c = 0.85 f_{cm}$
Tensile strength, f_t (MPa)	$f_t = 0.24 f_{cm}^{2/3}$
Elastic modulus, E_c (MPa)	$E_c = \left(6000 - 15.5 f_{cm}\right)\sqrt{f_{cm}}$
Fracture energy, G_f (MN/m)	$G_f = 0.000025 f_t$
Note: f_{cm} – mean concrete compressive strength	

625

626

627 **Table 4. Measured material properties**

Property	Mean	CoV
Cubic compressive strength (MPa)	62.8	3.2%
Fracture energy (N/m)	168	11.9%
Yield strength of reinforcement (MPa)	632	0.35%
Strain at yielding (‰)	2.83	8.45%
Tensile strength of reinforcement (MPa)	693	0.40%
Strain at ultimate (‰)	48.7	4.82%

628

629

630 **Table 5. Opening size summary**

Assigned number	Opening size ($L_0 \times H_0$)
0	No opening
1	0.9 m × 2.1 m
2	1.6 m × 2.1 m
3	3.0 m × 2.1 m
4	4.4 m × 2.1 m

631

632

633 **Table 6. Building model matrix relative to opening configuration**

Building		2nd Story				
		Solid	**Ox1**	**Ox2**	**Ox3**	**Ox4**
1st Story	**Solid**	AsBuilt	O01	O02	O03	O04
	O1y	O10	O11	O12	O13	O14
	O2y	O20	O21	O22	O23	O24
	O3y	O30	O31	O32	O33	O34
	O4y	O40	O41	O42	O43	O44

634

635

Table 7. Maximum reaction of wall D12

Reaction (MN)		2nd Story				
		Solid	**Ox1**	**Ox2**	**Ox3**	**Ox4**
1st Story	**Solid**	14.1 (0%)	12.7 (10%)	11.0 (22%)	8.8 (38%)	6.7 (52%)
	O1y	12.1 (14%)	11.8 (16%)	10.5 (26%)	8.4 (40%)	6.6 (53%)
	O2y	9.6 (32%)	9.8 (30%)	9.6 (32%)	8.2 (42%)	6.4 (55%)
	O3y	4.7 (67%)	5.3 (62%)	5.5 (61%)	6.2 (56%)	5.7 (60%)
	O4y	2.0 (86%)	1.8 (87%)	1.7 (88%)	1.8 (87%)	2.1 (85%)

639 **Table 8. Maximum uniformly distributed load applied to slabs in the critical bay**

Load (kN/m^2)		2nd Story				
		Solid	**Ox1**	**Ox2**	**Ox3**	**Ox4**
1st Story	**Solid**	201 (0%)	190 (5%)	149 (26%)	142 (29%)	185 (8%)
	O1y	192 (4%)	190 (5%)	146 (27%)	142 (29%)	152 (24%)
	O2y	178 (11%)	181 (10%)	184 (8%)	139 (31%)	151 (25%)
	O3y	91 (55%)	100 (50%)	119 (41%)	144 (28%)	181 (10%)
	O4y	61 (70%)	59 (71%)	58 (71%)	75 (63%)	84 (58%)

640

641

642 **Table 9. Maximum applied load from crack opening displacement criteria**

Load (kN/m^2)		2nd Story				
		Solid	**Ox1**	**Ox2**	**Ox3**	**Ox4**
1st Story	**Solid**	50	38	38	34	34
	O1y	44	38	38	37	34
	O2y	44	41	38	38	34
	O3y	44	37	34	37	37
	O4y	42	34	27	23	32

643

644

Table 10. Additional characteristic live load from serviceability conditions

Load (kN/m^2)		2nd Story				
		Solid	**Ox1**	**Ox2**	**Ox3**	**Ox4**
1st Story	**Solid**	33	25	25	22	22
	O1y	29	25	25	24	22
	O2y	29	27	25	25	22
	O3y	29	24	22	24	24
	O4y	27	22	17	15	21

Table 11. Maximum applied load from concrete crushing criteria

Load (kN/m^2)		2nd Story				
		Solid	**Ox1**	**Ox2**	**Ox3**	**Ox4**
1st Story	**Solid**	89	53	47	37	40
	O1y	53	56	47	37	40
	O2y	53	53	47	38	40
	O3y	44	40	43	34	37
	O4y	39	39	38	34	32

651 **Table 12. Maximum applied load from reinforcement yield criteria**

Load (kN/m^2)		2nd Story				
		Solid	**Ox1**	**Ox2**	**Ox3**	**Ox4**
1st Story	**Solid**	132	121	113	97	93
	O1y	130	125	118	108	93
	O2y	123	121	120	108	96
	O3y	91	76	77	87	97
	O4y	71	47	41	32	38

652

653

654 **Table 13. Building overload factor (OF)**

OF		2nd Story				
		Solid	**Ox1**	**Ox2**	**Ox3**	**Ox4**
1st Story	**Solid**	11.7	6.9	6.1	4.8	5.2
	O1y	6.9	7.3	6.1	4.8	5.2
	O2y	6.9	6.9	6.1	4.9	5.2
	O3y	5.7	5.2	5.6	4.4	4.8
	O4y	5.0	5.0	4.9	4.1	4.1

655

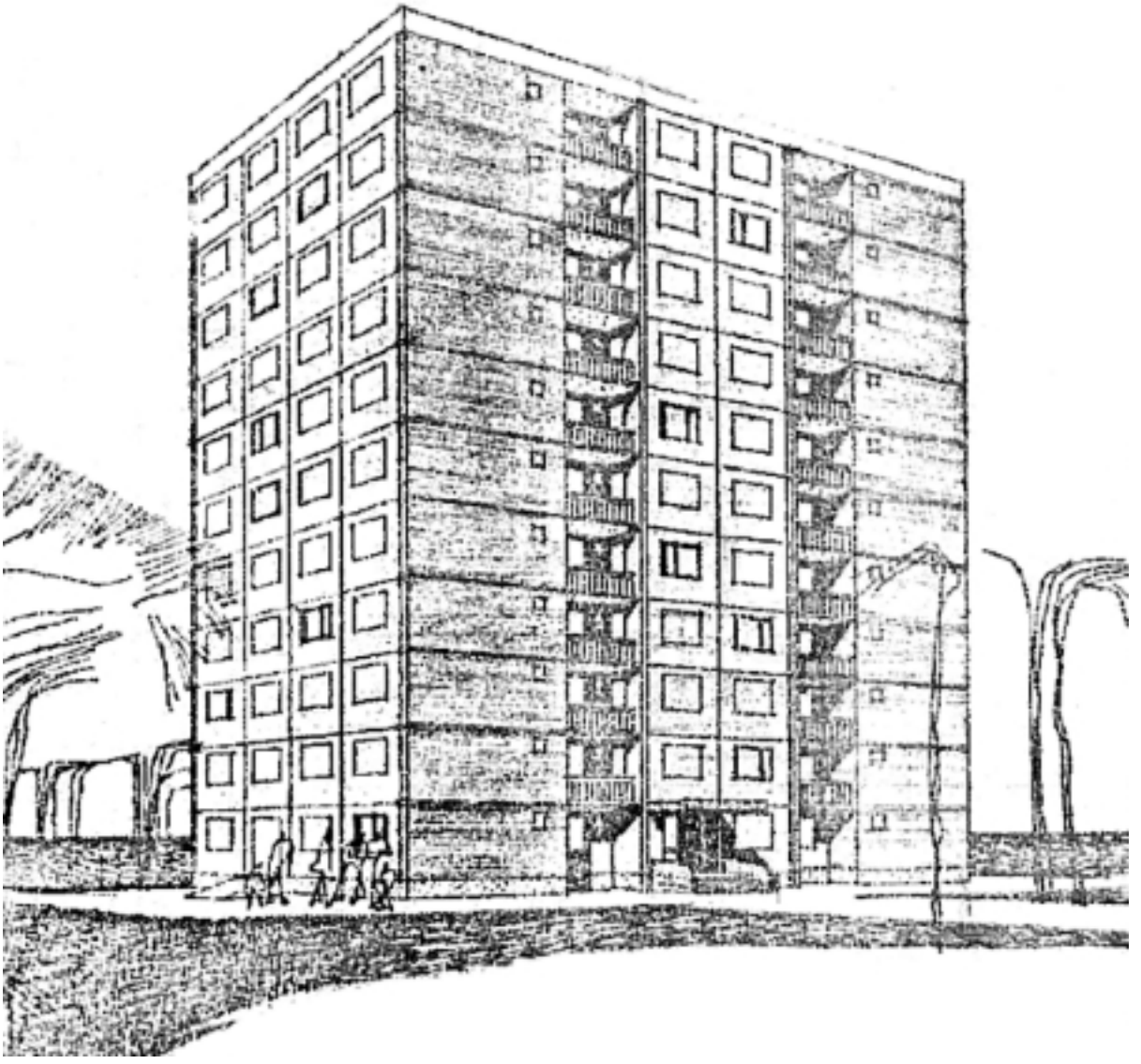

G
F
E
D
C
B
A
3.6
1.8
1.5
1.5
1.8
3.6
Wall 1BF
Wall 1DF
Slab E
Wall 2DF
cut-out openings
Wall D12
Wall 1BD
Slab C
Wall 2BD
5.4
3.3
3.3
1
2
3
4

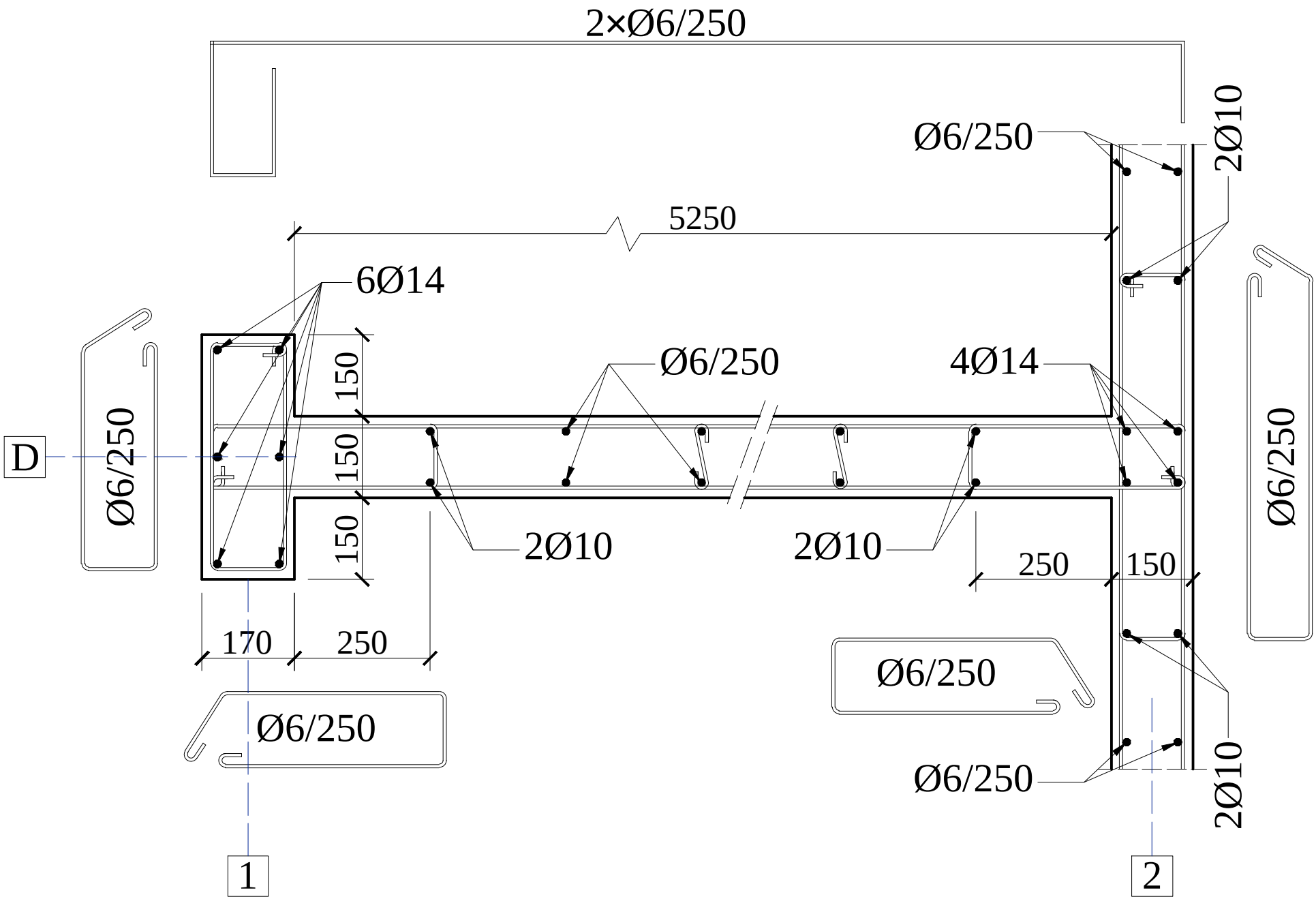
2×Ø6/250
Ø6/250
2Ø10
5250
6Ø14
Ø6/250
4Ø14
D
Ø6/250
150
150
150
2Ø10
2Ø10
250
150
Ø6/250
170
250
Ø6/250
Ø6/250
2Ø10
1
2

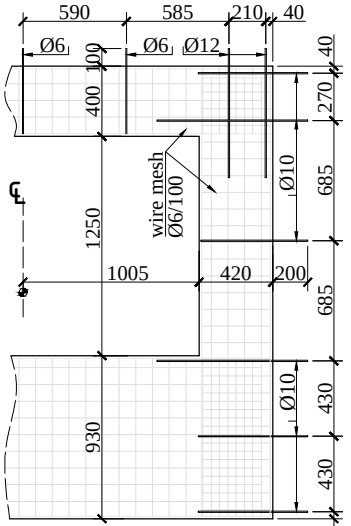
590
585
210
40
Ø6
Ø6
Ø12
100
400
270
Ø10
685
wire mesh
Ø6/100
1250
1005
420
200
685
Ø10
430
930
430
40

(a)

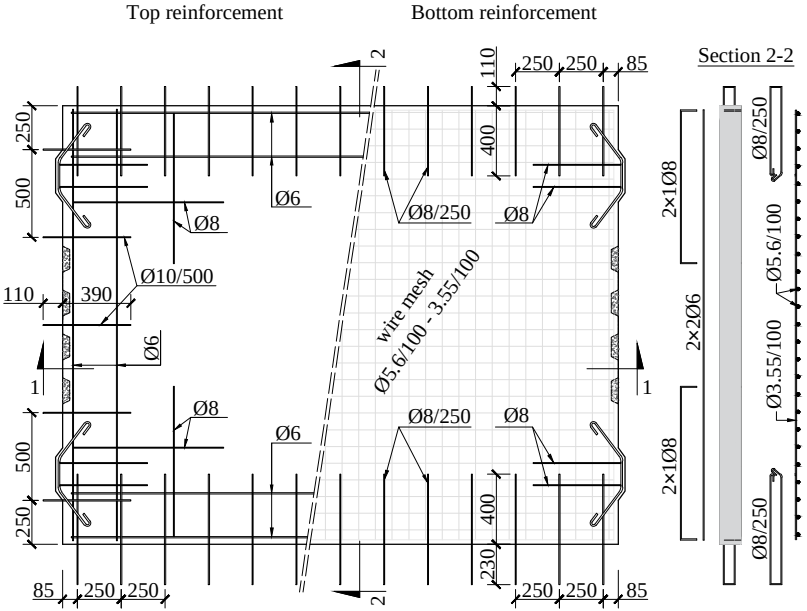
Top reinforcement
Bottom reinforcement
Section 2-2
2
110
250
250
85
250
500
Ø6
Ø8
Ø8/250
Ø8
400
Ø10/500
110
390
Ø6
wire mesh
Ø5.6/100 - 3.55/100
1
1
Ø8
Ø6
Ø8/250
Ø8
500
250
400
230
85
250
250
250
250
85
2×1Ø8
2×2Ø6
2×1Ø8
Ø8/250
Ø5.6/100
Ø3.55/100
Ø8/250

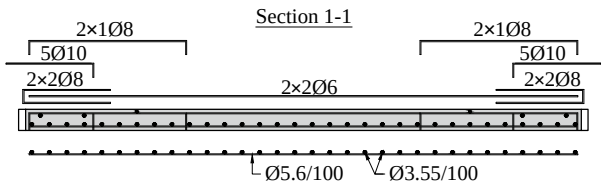
Section 1-1
2×1Ø8
5Ø10
2×2Ø8
2×2Ø6
2×1Ø8
5Ø10
2×2Ø8
Ø5.6/100
Ø3.55/100

(b)

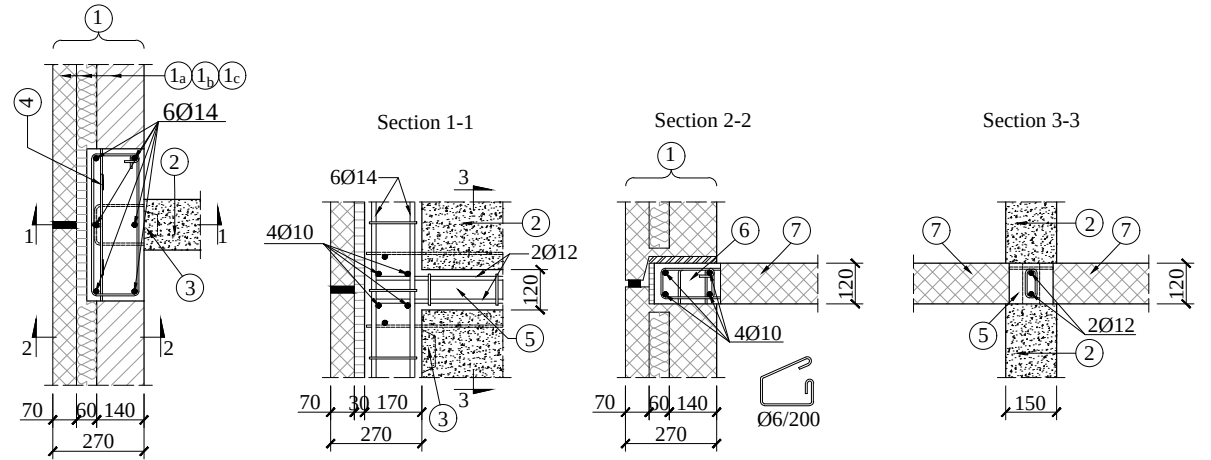

1 - prefabricated panel for outer walls (1_a - protective layer, 1_b - insulating material, 1_c - structural wall); 2 - cast-in-situ RC wall; 3 - shear key; 4 - lapped splices (dowels); 5 - tie-beam for inner walls; 6 - tie-beam for outer walls; 7 - prefabricated RC floor panel

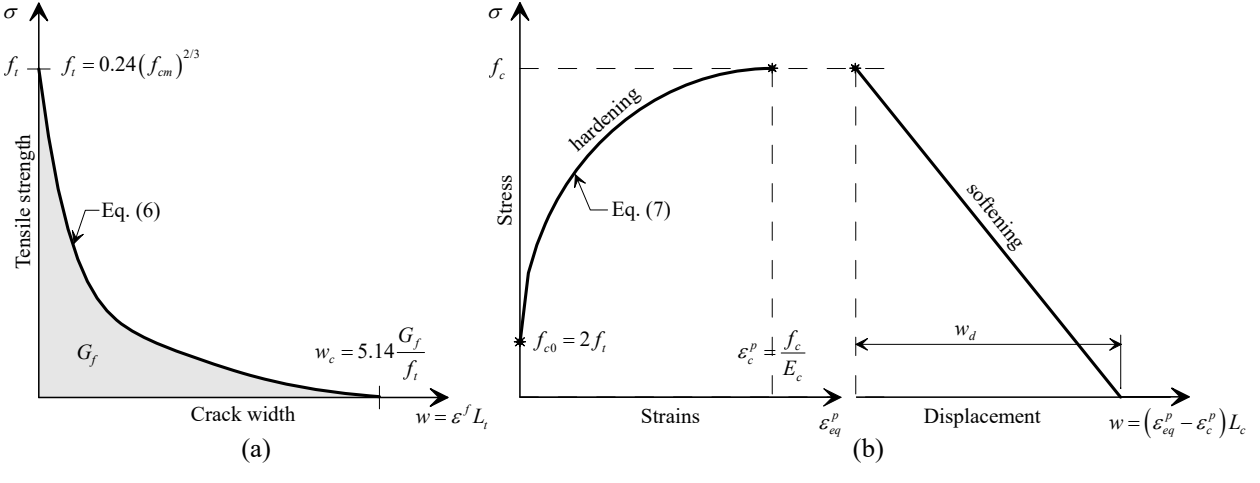
σ
f_t
$f_t = 0.24(f_{cm})^{2/3}$
Tensile strength
Eq. (6)
G_f
$w_c = 5.14\frac{G_f}{f_t}$
Crack width
$w = \varepsilon^f L_t$
(a)
σ
f_c
hardening
Eq. (7)
Stress
$f_{c0} = 2f_t$
$\varepsilon_c^p = \frac{f_c}{E_c}$
Strains
ε_{eq}^p
softening
w_d
Displacement
$w = (\varepsilon_{eq}^p - \varepsilon_c^p)L_c$
(b)

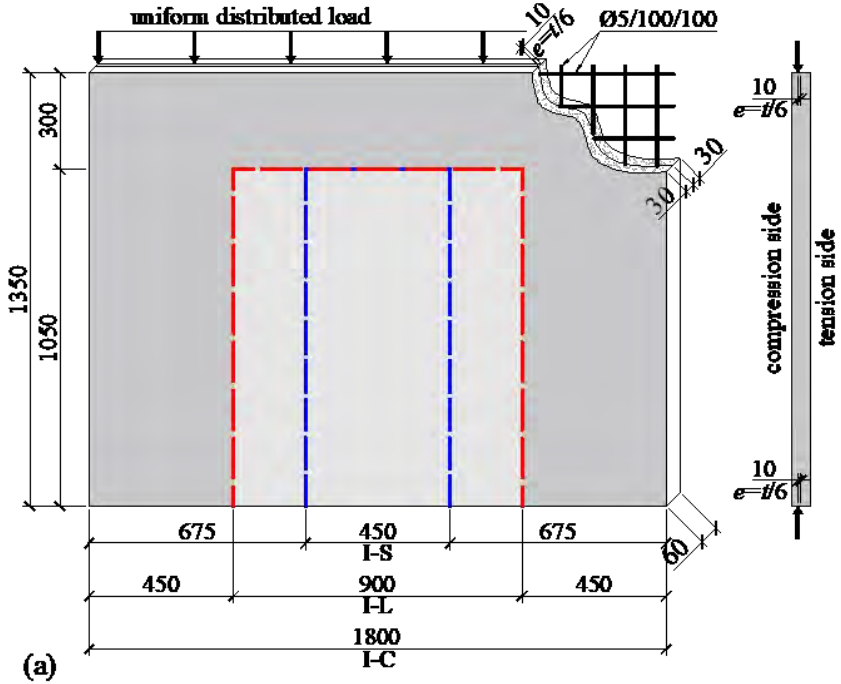
uniform distributed load
10
e=t/6
Ø5/100/100
300
1350
1050
30
30
10
e=t/6
compression side
tension side
10
e=t/6
675
450
675
I-S
450
900
450
I-L
1800
I-C
60
(a)

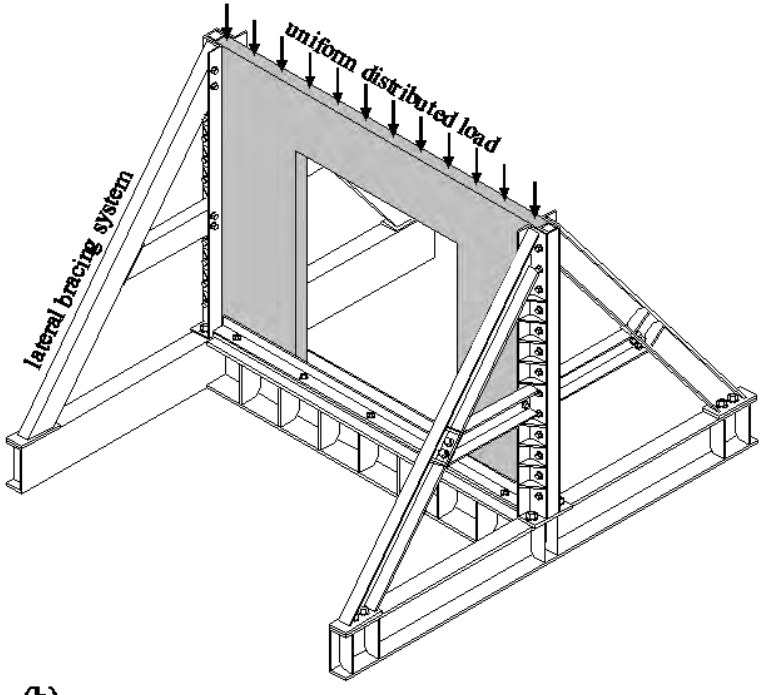
uniform distributed load
lateral bracing system
(b)

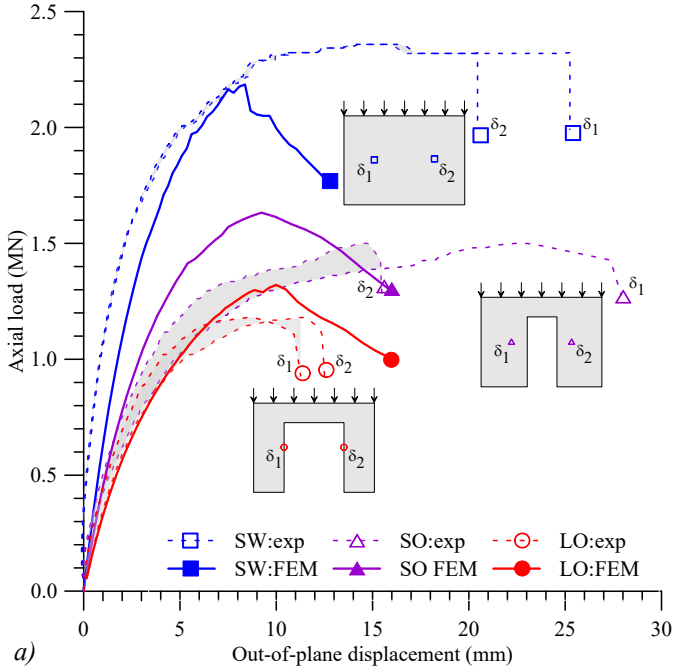
Axial load (MN)
Out-of-plane displacement (mm)
SW:exp
SW:FEM
SO:exp
SO FEM
LO:exp
LO:FEM
δ1
δ2

a)

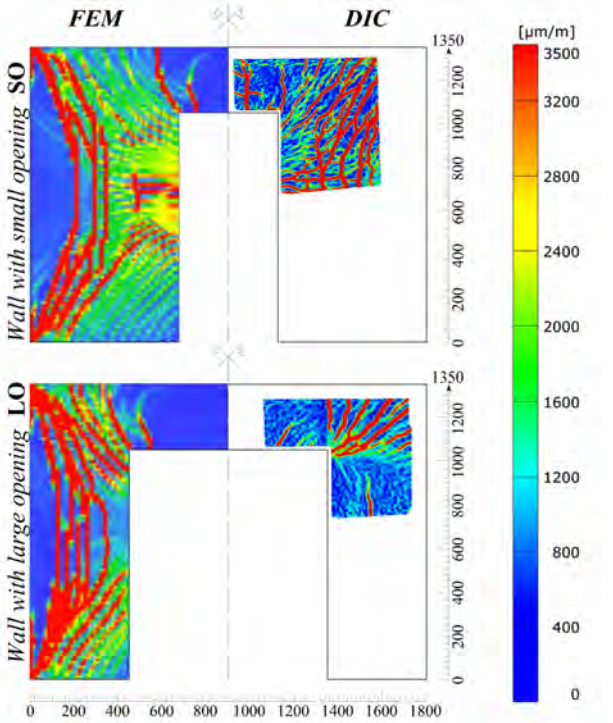
FEM
DIC
[μm/m]
Wall with small opening SO
Wall with large opening LO

b)

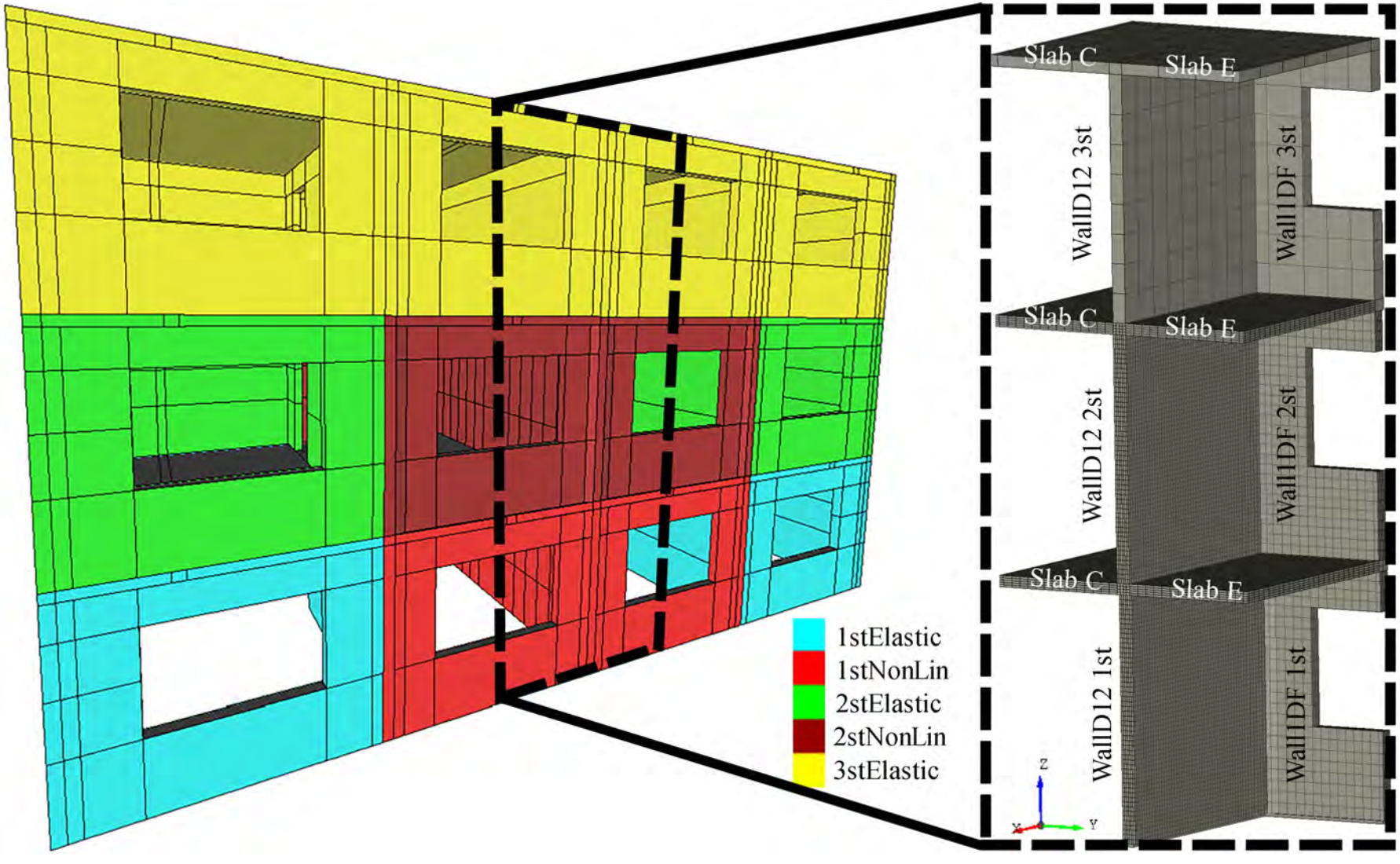
1stElastic
1stNonLin
2stElastic
2stNonLin
3stElastic
Slab C
Slab E
WallD12 3st
Wall1DF 3st
Slab C
Slab E
WallD12 2st
Wall1DF 2st
Slab C
Slab E
WallD12 1st
Wall1DF 1st
Z
Y
X

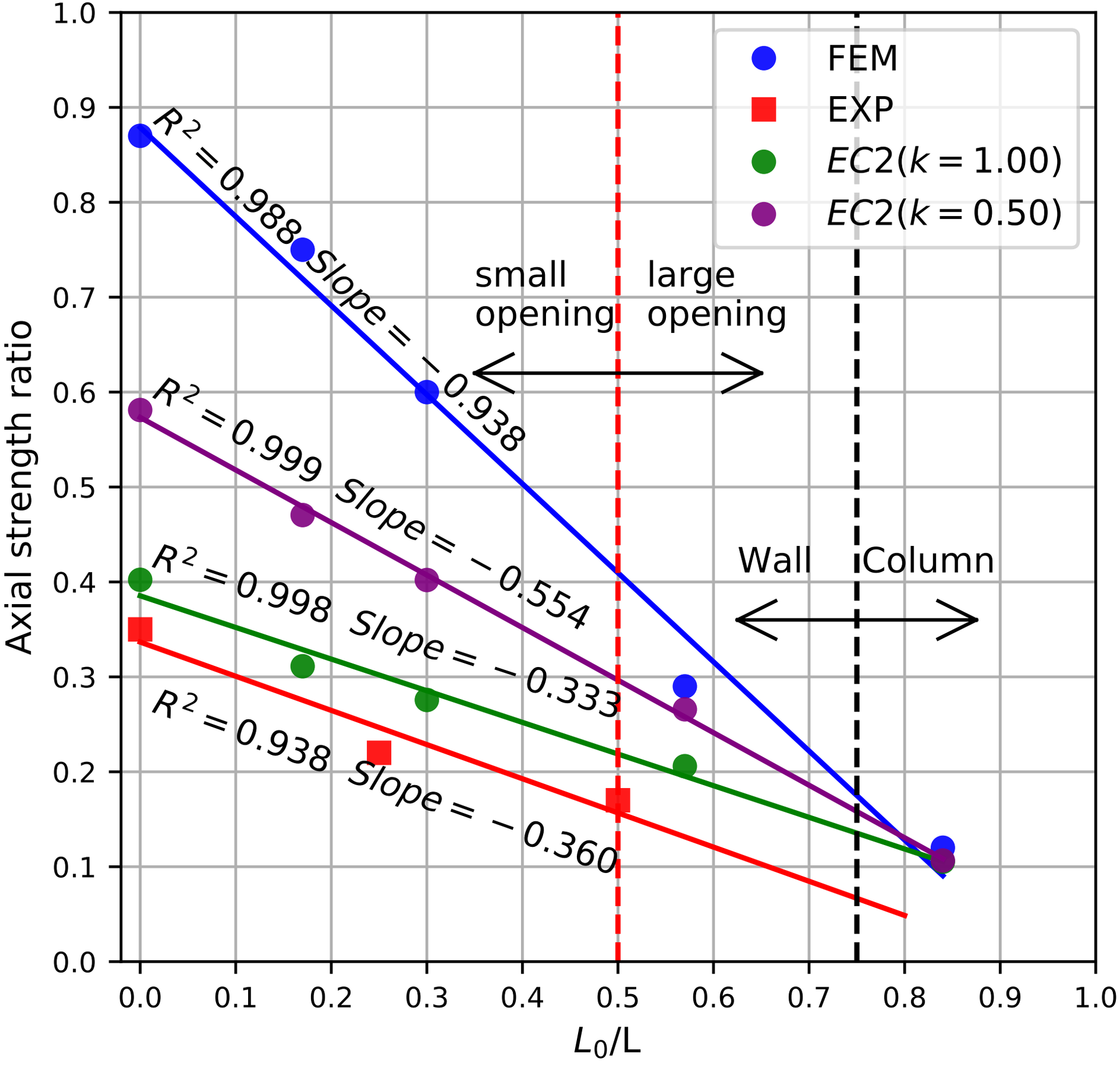
FEM
EXP
EC2(k = 1.00)
EC2(k = 0.50)
small opening
large opening
Wall
Column
R² = 0.988
Slope = −0.938
R² = 0.999
Slope = −0.554
R² = 0.998
Slope = −0.333
R² = 0.938
Slope = −0.360
Axial strength ratio
L0/L
0.0
0.1
0.2
0.3
0.4
0.5
0.6
0.7
0.8
0.9
1.0

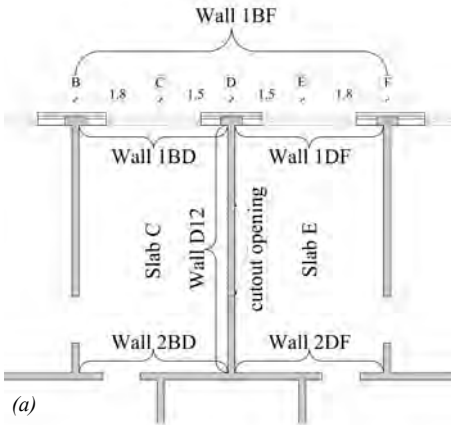
Wall 1BF
B
C
D
E
F
1.8
1.5
1.5
1.8
Wall 1BD
Wall 1DF
Slab C
Wall D12
cutout opening
Slab E
Wall 2BD
Wall 2DF

(a)

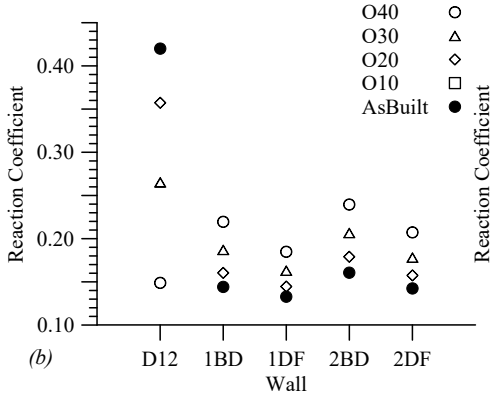
O40
O30
O20
O10
AsBuilt
Reaction Coefficient
0.10
0.20
0.30
0.40
D12
1BD
1DF
2BD
2DF
Wall

(b)

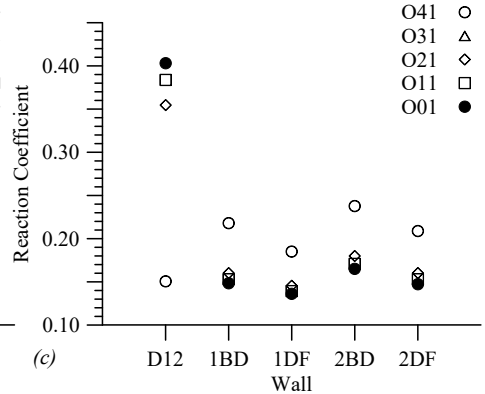
O41
O31
O21
O11
O01
Reaction Coefficient
0.10
0.20
0.30
0.40
D12
1BD
1DF
2BD
2DF
Wall

(c)

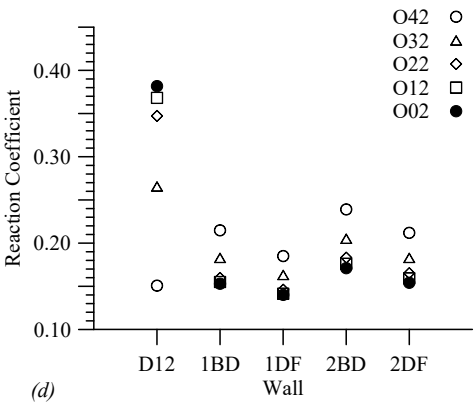
O42
O32
O22
O12
O02
Reaction Coefficient
0.10
0.20
0.30
0.40
D12
1BD
1DF
2BD
2DF
Wall

(d)

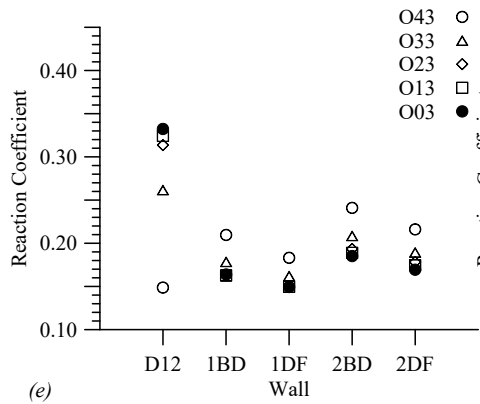
O43
O33
O23
O13
O03
Reaction Coefficient
0.10
0.20
0.30
0.40
D12
1BD
1DF
2BD
2DF
Wall

(e)

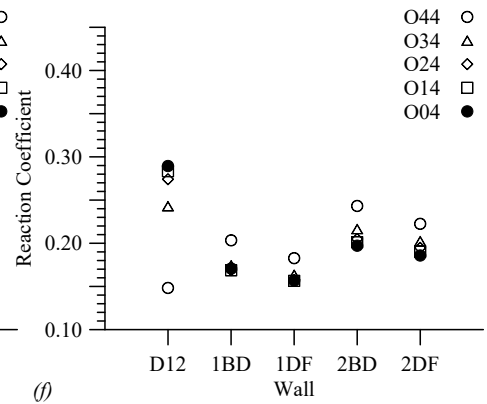
O44
O34
O24
O14
O04
Reaction Coefficient
0.10
0.20
0.30
0.40
D12
1BD
1DF
2BD
2DF
Wall

(f)

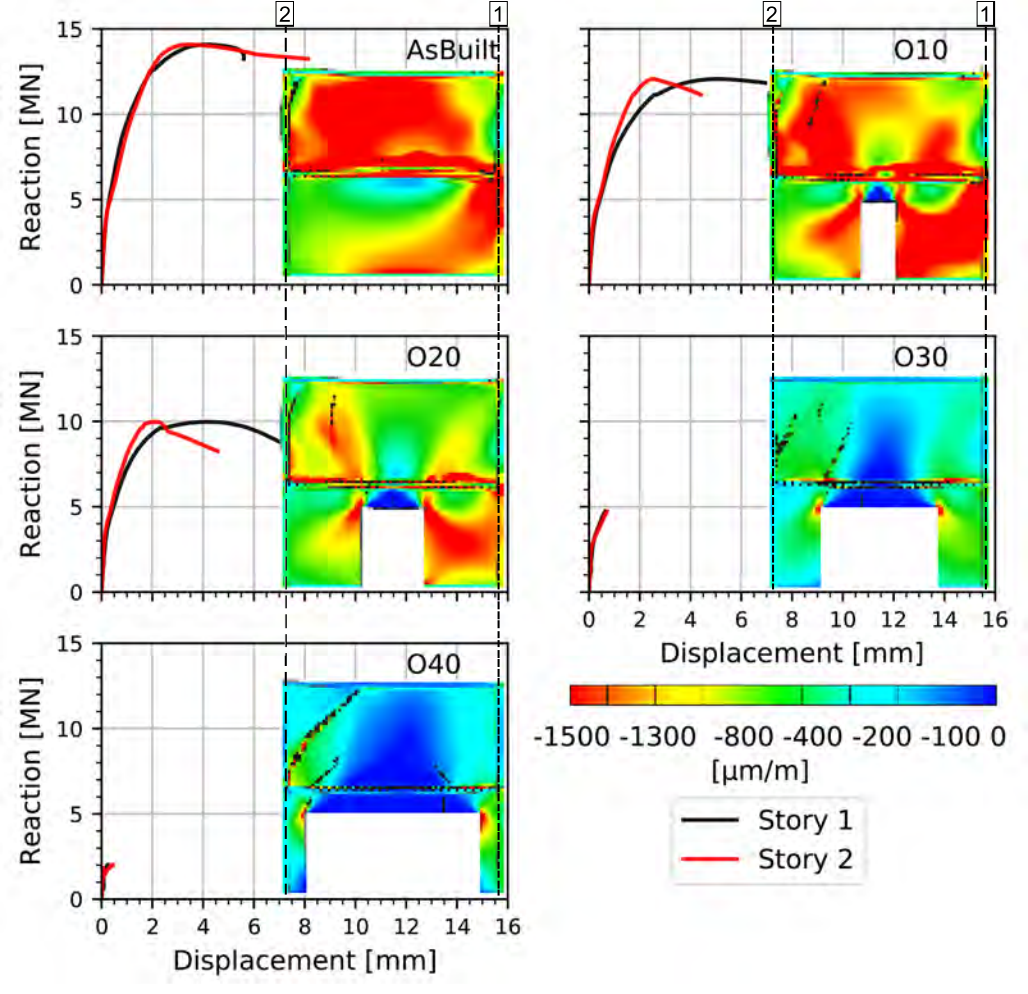
AsBuilt
O10
O20
O30
O40
Reaction [MN]
Displacement [mm]
2
1
-1500 -1300 -800 -400 -200 -100 0
[μm/m]
Story 1
Story 2

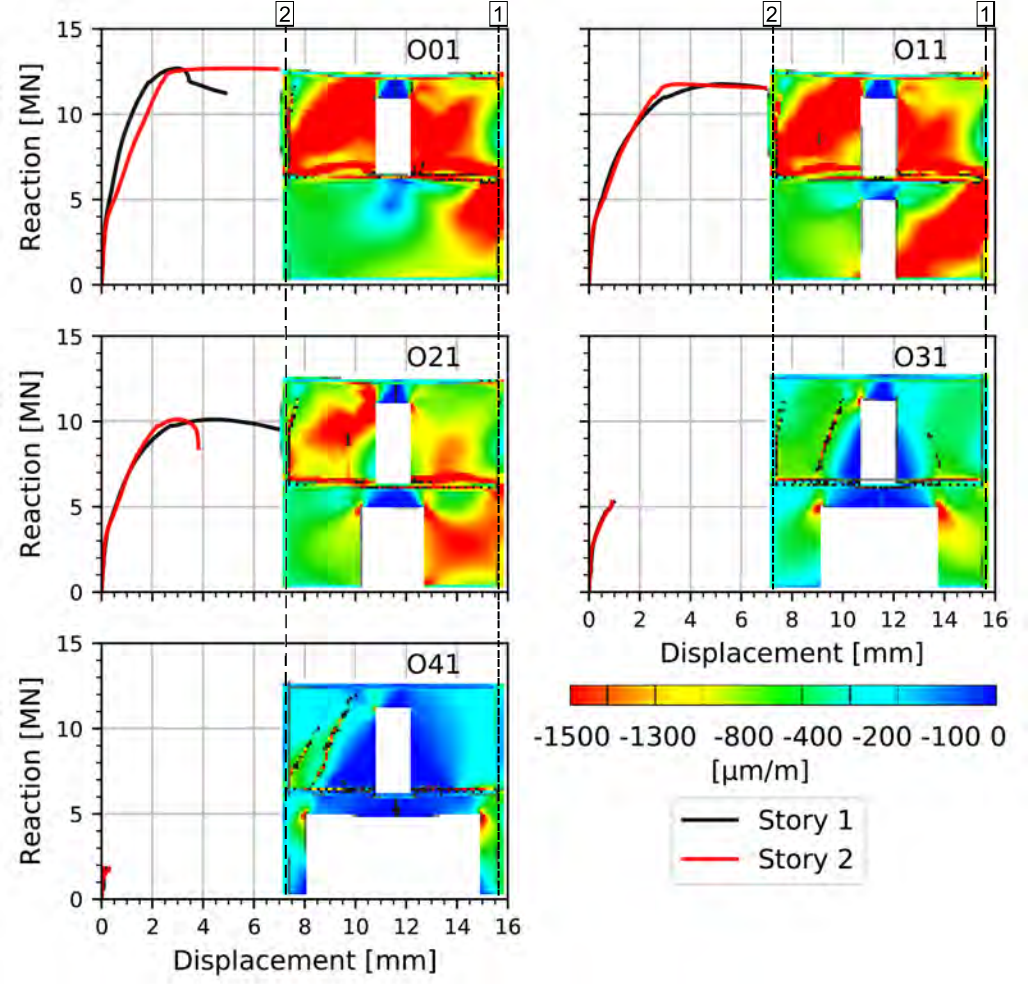
O01
O11
O21
O31
O41
2
1
Reaction [MN]
Displacement [mm]
-1500 -1300 -800 -400 -200 -100 0
[µm/m]
Story 1
Story 2

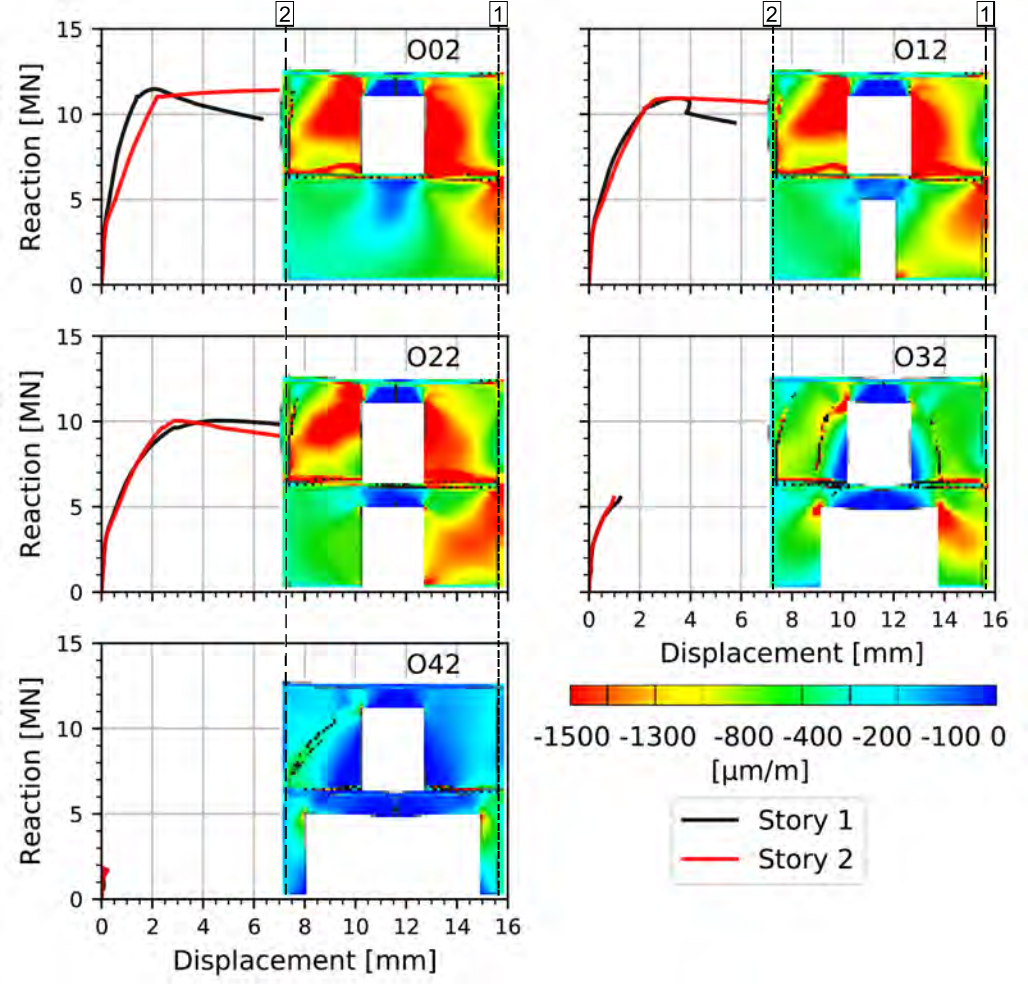
O02
O12
O22
O32
O42
2
1
Reaction [MN]
Displacement [mm]
0
2
4
6
8
10
12
14
16
5
15
-1500 -1300 -800 -400 -200 -100 0
[µm/m]
Story 1
Story 2

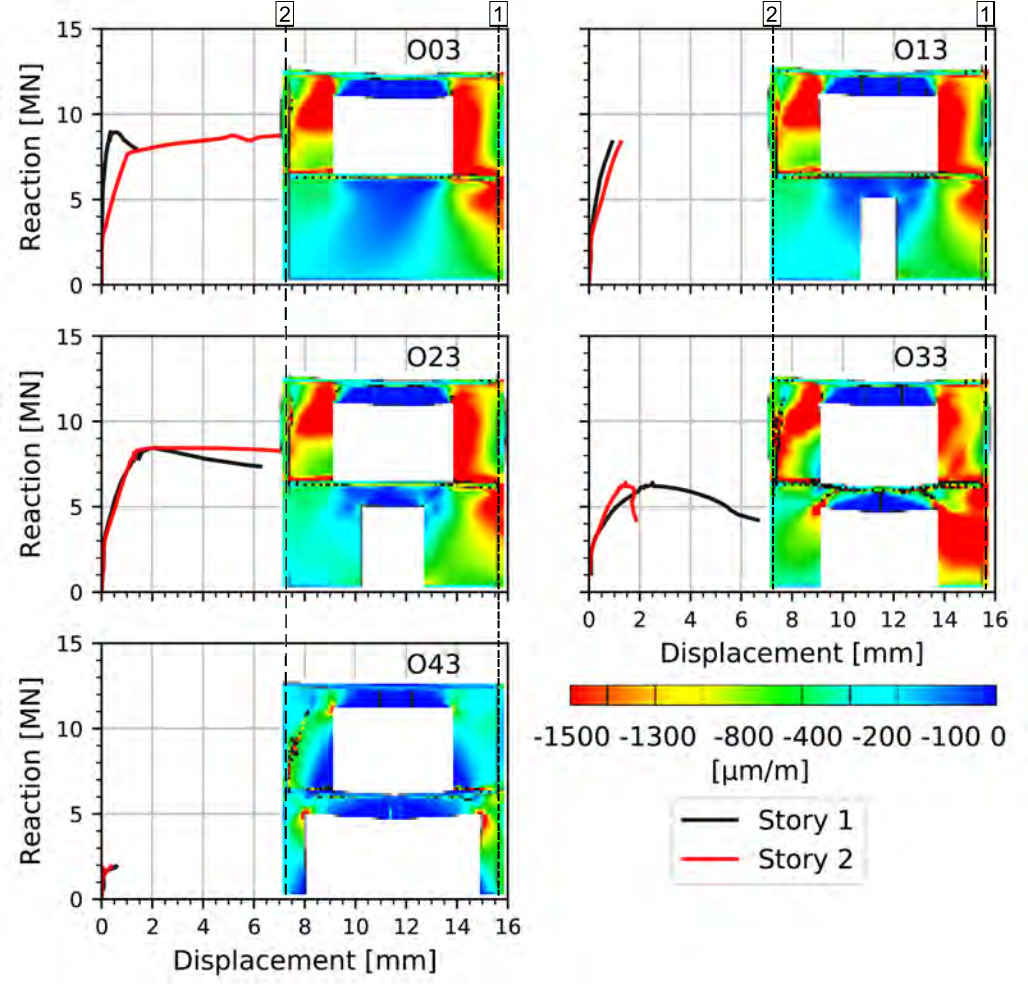
O03
O13
O23
O33
O43
2
1
Reaction [MN]
Displacement [mm]
0 2 4 6 8 10 12 14 16
0 5 10 15
-1500 -1300 -800 -400 -200 -100 0
[µm/m]
Story 1
Story 2

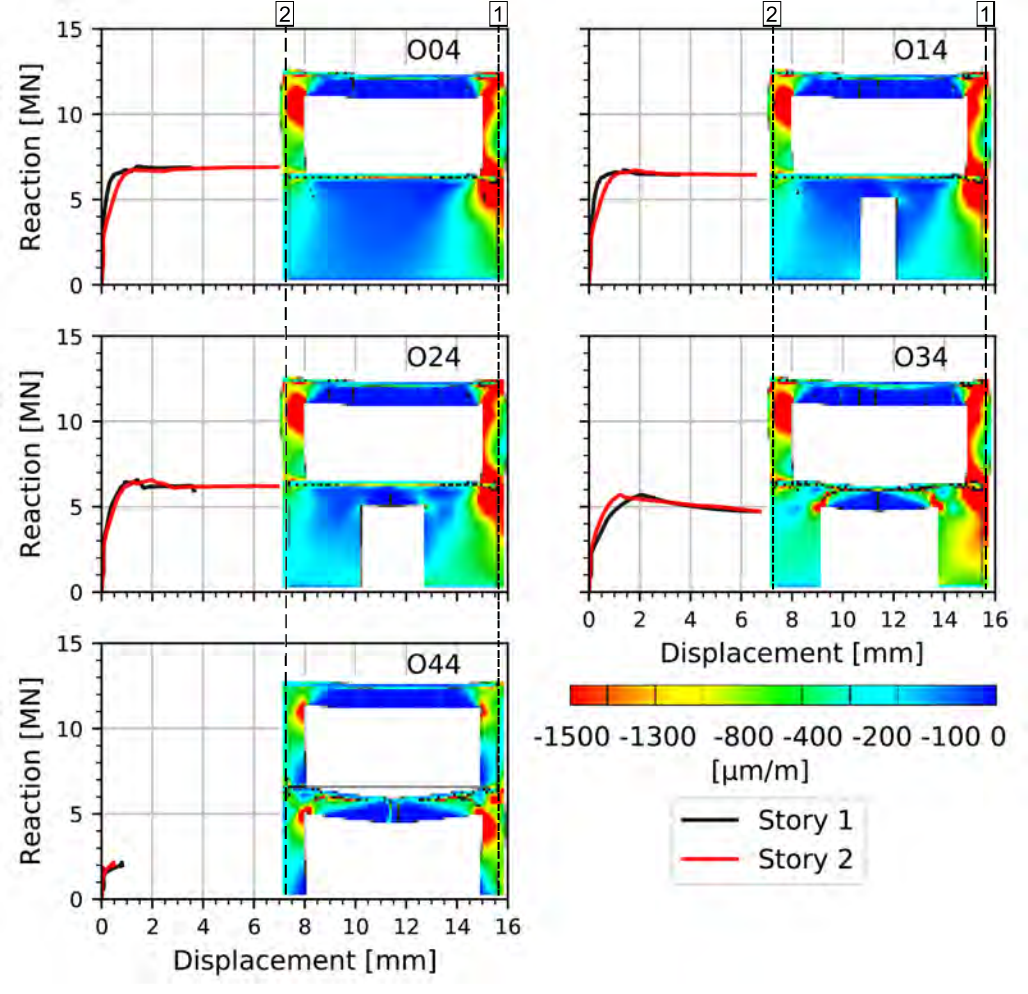
O04
O14
O24
O34
O44
2
1
Reaction [MN]
Displacement [mm]
0
2
4
6
8
10
12
14
16
5
15
-1500 -1300 -800 -400 -200 -100 0
[µm/m]
Story 1
Story 2

The authors declare that they have no conflict of interest.